ROYAL SOCIETY OF CHEMISTRY

REVIEW

Check for updates

Covalent triazine frameworks for carbon dioxide capture

Han Wang, [ab] Danni Jiang, [ab] Danlian Huang, [ab] Guangming Zeng, [*ab] Piao Xu, [*ab] Cui Lai, [ab] Ming Chen, [ab] Min Cheng, [ab] Chen Zhang [ab] and Ziwei Wang [ab]

Since the industrial revolution, the concentration of atmospheric greenhouse gases especially CO_2 released by human activity is increasing year by year, leading to a series of serious problems such as global warming and climate change. Finding a way to mitigate this dilemma is of crucial importance. Covalent triazine frameworks (CTFs), as a new class of porous materials, have gained considerable attention due to their attractive chemical and structural merits. They show great potential for various applications especially for CO_2 capture. In this review, we aim to provide recent advances in using CTFs for CO_2 capture. First, a brief background is provided including a summary statement on the current situation of the CO_2 issue, a general overview of typical porous materials used in CO_2 capture, and an introduction to CTFs. Second, synthetic reactions and methods related to CTFs are summarized and compared, and a short discussion of characterization methods is provided. Furthermore, CO_2 capture performance including CO_2 adsorption at low/high-pressure, gas selectivity, heat of CO_2 adsorption, recyclability and CO_2 capture of CTFs in a humid atmosphere is elucidated on the basis of CTF design. Then, strategies for enhancing the CO_2 adsorption ability of CTFs based on pore engineering and surface functionalization are given. Finally, a perspective of CTFs for CO_2 capture is presented.

1. Introduction

With population growth and industrial development, one of the most serious problems facing the world is global warming which has widespread influences on human and natural systems. According to data obtained from the National Oceanic and Atmospheric Administration (NOAA), the average global temperature of the land and ocean surface in 2017 was 0.84 °C higher than that of the twentieth century (Fig. 1a).[1] The

aCollege of Environmental Science and Engineering, Hunan University, Key Laboratory of Environmental Biology and Pollution Control (Hunan University), Ministry of Education, Changsha, Hunan 410082, PR China. E-mail: zgming@hnu.edu.cn; piaoxu@hnu.edu.cn; Fax: +86-731-88823701; Tel: +86-731-88822754

bKey Laboratory of Environmental Biology and Pollution Control, Ministry of Education, Hunan University, Changsha 410082, P. R. China

Han Wang received her M.E. from the Chinese Academy of Science in 2016. Currently, she is a PhD candidate under the supervision of Prof. Guangming Zeng in College of Environmental Science and Engineering, Hunan University, China. Her current research interests focus on the synthesis and application of functional covalent organic materials.

Prof. Guangming Zeng teaches courses and performs research on environmental science and health at Hunan University since 1988. He has been the head of the School of Environmental Science and Engineering since 1994 at the same university. He is one of the 2017 Highly Cited Researchers in the world issued by Clarivate Analytics. His current research interests focus on the synthesis and application of functional nanomaterials in the field of environment and energy.

increased emission of carbon dioxide (CO_2), mainly originating from the burning of fossil fuels in power plants or industrial manufacturing, is deemed as one of the chief culprits of the problem (Fig. 1b). Thus, how to efficiently reduce the CO_2 emission is attracting considerable attention. Carbon capture and storage (CCS) is widely regarded as a potential strategy to achieve the target of CO_2 removal. Generally, a three-step CCS method including CO_2 capture, transportation and permanent storage is employed. While technologies of CO_2 transportation and storage are widely studied and lots of them have met the requirements for commercialization, those of CO_2 capture are still far from being developed. The high cost and large energy consumption of CO_2 capture are impeding the deployment of CCS practical applications.

1.1. Technologies in CO_2 capture

Using clean energy with few or no carbon content like hydrogen technology is the best strategy, but it is still far from sufficiently developed. Thus, reducing CO_2 generation from the source such as power plants and industrial operation seems to be the most direct way to lower the level of anthropogenic CO_2 in the atmosphere. Based on the emission of CO_2, several cost-effective and scalable technologies have been developed, namely pre-combustion capture, post-combustion capture, and oxy-fuel combustion (Fig. 2).[2,3]

Piao Xu received her Ph.D degree from the College of Environmental Science and Engineering, Hunan University, in 2016. She is currently a professor in the College of Materials Science and Engineering, Hunan University. Her major research focus is on the development of nanomaterials and application in environmental remediation.

**Top (from left to right): Danlian Huang; Lai Cui; Ming Chen
Bottom (from left to right): Chen Zhang; Min Cheng;
Danni Jiang; Ziwei Wang**

Pre-combustion capture means conversion before separating CO_2. O_2 or air is provided to the system to react with the primary fuel to produce H_2. Generally, the synthesis gas (syngas) composed of CO and H_2 is obtained because of an incomplete reaction. Hence, a shift converter, which enables CO to further react with stream to produce CO_2 and involves more H_2, is needed followed by various technologies to separate CO_2 and H_2.[4] While pre-combustion requires lower energy, the efficiency and temperature with respect to H_2-rich gas turbine fuel might be a bit challenging. Moreover, the issues including the substantial capital cost and public resistance for new construction also exist. Alternative methods such as chemical looping cycles need to be studied to generate syngas.[5]

Contrast to pre-combustion capture, post-combustion capture relies on the separation of CO_2/N_2 from exhaust flue gas before releasing to the atmosphere. The relatively low CO_2 concentration in combustion flue gas along with atmospheric pressure and temperature of 40–150 °C makes the process efficient.[6,7] In addition, flue gases can be reused by the existing power plants using various technologies.[8] For example, bioreactors can be fed using cooled and CO_2-rich flue gases to produce microalgal biomass indicating that flue gases can be utilized as biofuel.[9–11] Furthermore, a unique strength of this technique is that the system can continue to generate electricity in case of shutting down the CO_2 capture unit for an emergency.

Compared to the first two approaches, oxy-fuel combustion has the advantage of producing almost pure CO_2 with almost pure O_2 instead of air to combust the fuels, which enables direct storage.[12] But the disadvantage of this approach is the essential prerequisite of pure O_2 that is usually obtained from air separation, which needs high capital cost.

1.2. Materials in CO_2 capture

As mentioned above, the technologies of adsorption and separation for CO_2 capture seem to be the biggest challenge and sorbents with high performance are needed to be urgently designed and developed. Among the technologies used in CO_2 capture systems, chemical adsorption with aqueous amine solutions has met the commercial criterion.[13] However, there are major drawbacks which greatly increase the running cost of power plants. For example, costly design for durability and frequent housekeeping for safe running are necessary considering as the amine solutions and vapors may cause equipment corrosion.[14] In addition, separating CO_2 from the sorbents needs a large quantity of energy, which also makes aqueous amine solutions uneconomical.[8]

Besides chemisorption, physisorption in porous materials has been considered as an attractive alternative because of its reversible process and smaller energy requirements. Several classes of porous materials including zeolites,[15,16] porous carbons[17–20] and MOFs[21–24] are deemed to be promising candidates in CCS applications as they have the merits of large CO_2 adsorption capacity, high CO_2 selectivity, good stability and regeneration. Moreover, mechanical robustness, pore size and pore surface engineering are important to consider. For example, zeolites, with low production cost, high thermal and
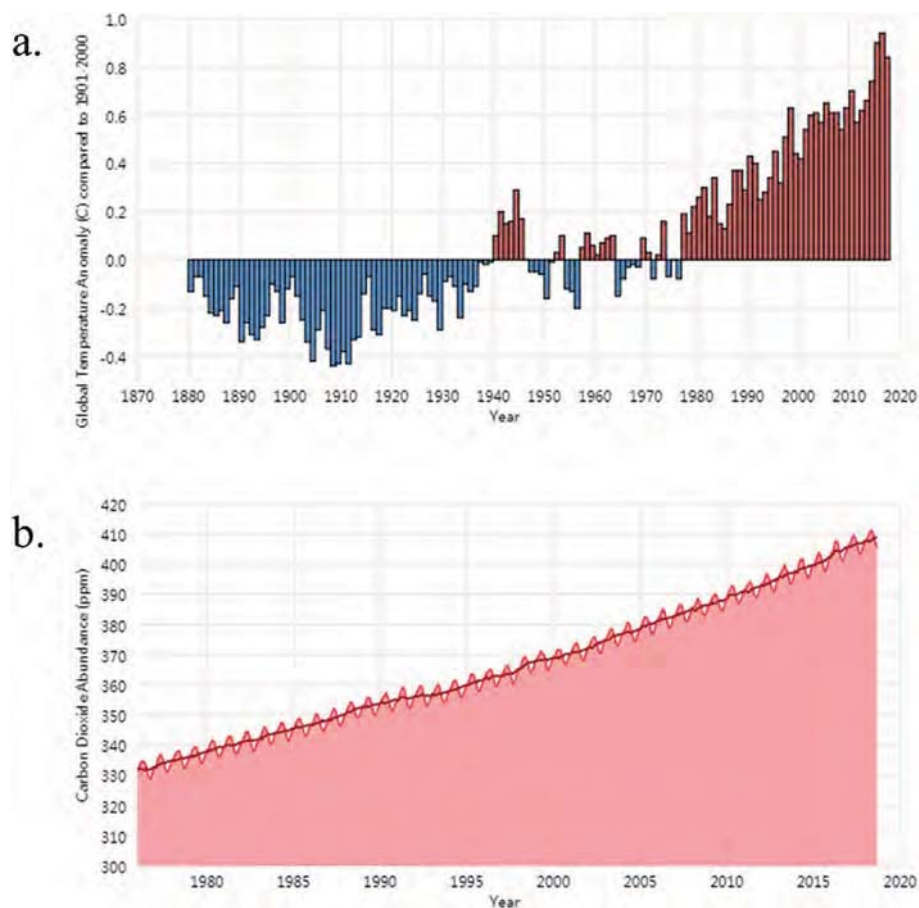
This journal is © The Royal Society of Chemistry 2019

J. Mater. Chem. A, 2019, **7**, 22848–22870 | **22849**

Fig. 1 (a) History of global surface temperature since 1880; (b) increased atmospheric CO_2 concentration measured during 1980–2017 at NOAA's Mauna Loa Observatory in Hawai'i. Reproduced with permission from ref. 1. Copyright 2017, NOAA Climate.gov.

chemical stability, high mechanical robustness and structural diversity, are regarded as strong candidates for CO_2 capture with good capacity and selectivity.[25] However, poor performance under humid conditions, high energy cost of regeneration, small high-pressure CO_2 capture capacity, and difficulties in accurate functionalization and structural adjustment impede further development.[26] Activated carbons are another porous material which have good high-pressure CO_2 capture capacity and retain high performance even in a humid environment.[27–29] But major bottlenecks such as poor CO_2 selectivity, weak low-
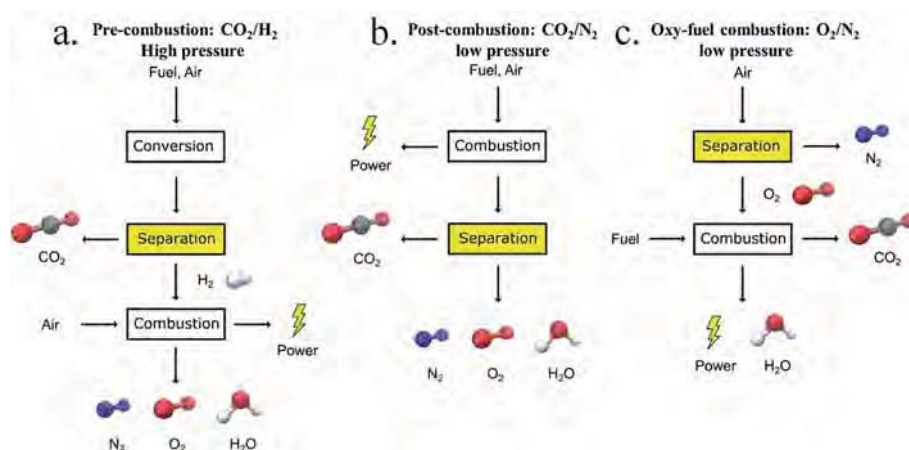

Fig. 2 Representative scheme of CCS strategies: (a) pre-combustion; (b) post-combustion; (c) oxy-fuel combustion. Reproduced with permission from ref. 2. Copyright 2018, American Chemical Society.

pressure working capacity, out-of-order pore width, and difficulties in pore engineering greatly make their application restricted. MOFs with great structural tunability and high porosity are identified as another ideal platform for CO_2 capture.[30,31] Compared to the above mentioned materials, characteristics such as capacity for pore functionalization endow some MOFs with relatively high CO_2 capture performance.[32–34] However, in some cases, the CO_2 capture performance of MOFs is closely correlated with their open metal sites, which preferentially bond with H_2O stronger than with CO_2 and thus become unstable in humid gas mixtures. Peculiarly, even the MOFs with the best performance face the challenge of recyclability in the presence of water.[35,36] In addition, their relatively weak mechanical robustness also impedes the practical application in CO_2 capture.[37]

1.3. Covalent triazine frameworks

As a newly emerging class of porous materials, covalent organic frameworks (COFs) have attracted much attention in the area of CO_2 capture.[38] On the one hand, COFs possess some similar characteristics to MOFs such as high CO_2 adsorption and selectivity, high structural tenability, and easy regeneration. On the other hand, COFs gain an advantage over MOFs because they can maintain the high CO_2 capture capacity under humid conditions. Covalent triazine frameworks (CTFs) are known as a subclass of COFs with a triazine core having been widely studied in CO_2 capture because of the nitrogen-rich nature. Interestingly, the discovery of CTFs may date back to 1973, while their growth was large after the year 2008 with the work done by Kuhn and co-workers.[39] A series of CTFs with varied monomers were first systematically designed and constructed using ionothermal synthesis. Generally, CTFs are frameworks containing triazine units linked by covalent bonds which possess advanced stability compared to many coordinative-linked materials. The triazine unit can be formed in the trimerization reaction or simply originate from the building blocks. At the outset, CTFs were synthesized by the trimerization reaction under ionothermal conditions with the catalysis of $ZnCl_2$. Soon after, some other construction approaches such as trifluoromethanesulfonic acid (TFMS) catalyzed condensation, Schiff-base reaction, and Friedel–Crafts reaction have been introduced. Notably, the crystallinity of CTFs usually depends on the synthesis methods and conditions.

Different from the above mentioned traditional crystalline porous solids, CTFs with precisely targeted, controllable and predictable synthesis are able to achieve pre-designable structural and chemical properties specific to functions. In addition, they have a high nitrogen content which can enhance CO_2 capture by physisorption π systems. These along with the high surface area, tunable pore size, and low density endow them with an extremely wide scope of application potential especially in CO_2 adsorption. Specifically, in some cases, CTFs with an ultra-high surface-area show weak physical interactions with CO_2, and they have been used in pre-combustion carbon capture under elevated pressures. The functional engineering of CTFs with polar groups, such as inorganic ions, oxygen-rich groups, and nitrogen-rich groups, can help strengthen the average dipole–quadruple interactions with CO_2 molecules, thus improving the CO_2 capacity.

With the development of CTFs, while several reviews related to CTFs and their applications have been published,[40–42] reviews specific to CO_2 capture are rare. In this review, a comprehensive summarization of CO_2 capture using CTFs is provided for the first time and is classified into the following sections based on the synthesis of CTFs and their application in CO_2 capture: (1) the synthesis reaction and conditions of CTFs are summarized including the trimerization reaction, Schiff-base reaction, Friedel–Crafts reaction, nucleophilic substitution reaction and so on; (2) the characterization of CO_2 capture performance and the relationship between the chemical and structural natures of CTFs and their adsorption capacities are provided; (3) strategies for enhancing the CO_2 adsorption ability of CTFs are listed systematically including controlling the pore size and surface area, functionalization of the pore wall and optimization of the technical procedure; and (4) a brief conclusion and perspective for using CTFs for CO_2 capture are also discussed regarding further development.

2. Synthetic reactions and methods of CTFs

One of the greatest strengths of CTFs is the tailor-made building blocks and optional synthetic routes. To date, a significant amount of stable CTFs with different topologies have been synthesized with various methods. Usually, the trimerization reaction catalyzed by $ZnCl_2$ or CF_3SO_3H is the most extensively used method for the production of porous and stable CTFs. Nevertheless, other reactions have also been utilized including Schiff-base reaction, Friedel–Crafts reaction, nucleophilic substitution reaction, Yamamoto coupling reaction and so on. Herein the progress in the synthesis of CTFs is summarized.

2.1. Trimerization reaction

The vast majority of CTFs obtained *via* the trimerization reaction have been prepared under ionothermal conditions catalyzed by $ZnCl_2$ or trifluoromethanesulfonic acid (TFMS). The molten $ZnCl_2$ salt in the reaction can act as the solvent and catalyst for the reversible cyclotrimerisation reaction, and strong Brønsted acids such as TFMS also can be used as the catalyst related to the trimerization of nitriles.[43,44]

2.1.1. $ZnCl_2$-based trimerization reaction. Early in 2008, Thomas and co-workers pioneered a way to synthesize porous CTFs *via* a $ZnCl_2$-based trimerization reaction.[39] A series of nitrile building units, such as 1,4-dicyanobenzene and 2,6-dicyanopyridine, were employed to carry out trimerization in the presence of molten $ZnCl_2$ at 400 °C to afford black CTFs (Fig. 3, taking CTF-1 as an example). The as-prepared CTFs showed high chemical and thermal stability. Usually, a higher ratio of $ZnCl_2$ and monomers yields highly porous yet amorphous materials.[45–49] And longer reaction time which enables the reversible and self-repairing formation of triazine rings leads to increased crystallinity.[50] However, only a few crystalline

This journal is © The Royal Society of Chemistry 2019

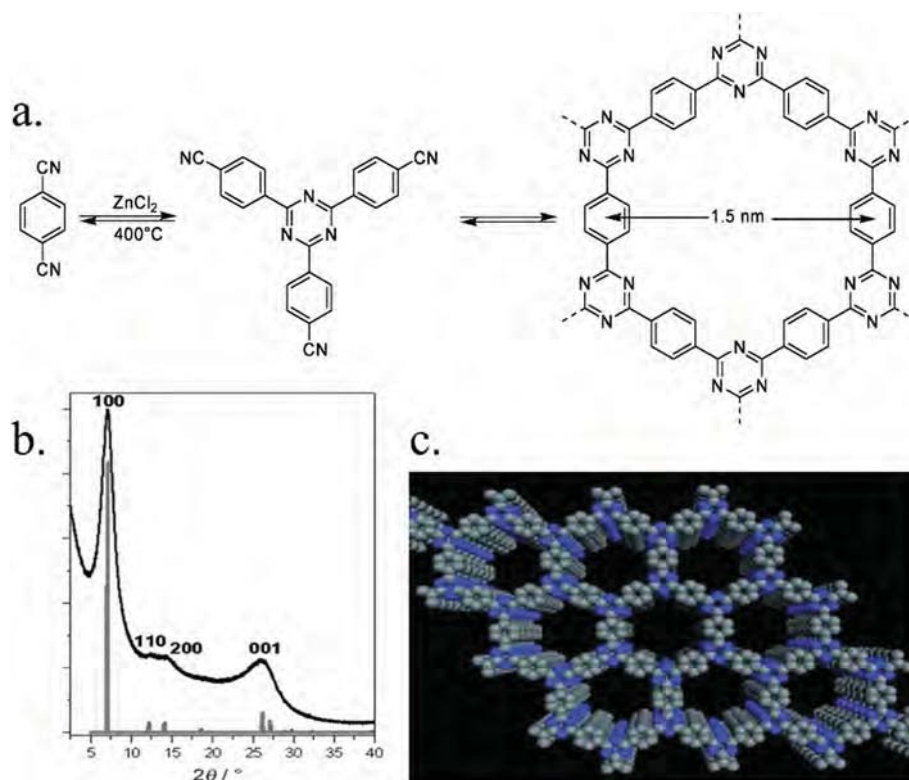J. Mater. Chem. A, 2019, 7, 22848–22870 | 22851

Fig. 3 (a) Representative synthetic route of CTF-1; (b) XRD pattern of CTF-1; (c) structure of CTF-1. Reproduced with permission from ref. 39. Copyright 2008, Wiley-VCH.

CTFs have been reported using this approach namely CTF-0,[50] CTF-1 [39] and CTF-2 [49] based on 1,3,5-tricyanobenzene, 1,4-dicyanobenzene and 2,6-dicyanonaphthalene monomers, separately. Several studies demonstrated that carbonization would occur in the reaction process especially at a high temperature (400–600 °C) and high $ZnCl_2$/monomer ratio, which caused the collapse of the structure and realized extended pore apertures.[51,52] Considering a high temperature of about 400–700 °C and long reaction time of 20–116 h for the condensation of nitriles under conventional ionothermal conditions, Qiu and co-workers presented a microwave (MW)-enhanced ionothermal method for energy-saving and highly effective synthesis of CTFs.[53,54] CTF with a high surface area could be obtained easily in tens of minutes and higher MW power and longer reaction time led to a higher BET surface area of CTFs in a certain range. Notably, all of the CTF materials synthesized by the MW-assisted method were amorphous, and all the samples exhibited a type IV isotherm, indicating the structure of micropores with mesopores formed by the close-packed nanoparticles.[55] In this MW-enhanced synthesis, samples with high porosities (up to 2.52 cm^3 g^{-1}) and surface areas (up to 2390 m^2 g^{-1}) could be easily realized within 10–60 min at a lower MW power output (280 W). To solve the problems of existence of thermal decomposition and acidolysis during the trimerization reaction and the difficulty in removing the $ZnCl_2$ catalyst, Wang and co-workers further developed a consolidated ionothermal strategy to synthesize CTFs by the condensation of

thermally unstable nitriles instead of the traditional one-step procedure.[56] Another similar strategy named multiple-step heating program was applied to synthesize a series of porous triazine-based polyimide networks (TPIs@IC) which proved to be useful for synthesizing CTFs from thermal/chemical unstable monomers.[57] For example, with a given molar ratio of $ZnCl_2$ and monomers (10 : 1), TPI-1@IC was synthesized through a selected temperature program (200 °C/5 h, 300 °C/5 h, and 400 °C/20 h), while TPI-2@IC was obtained through a temperature program (200 °C/5 h, 300 °C/5 h, 400 °C/10 h, 450 °C/10 h, and 500 °C/20 h). The BET surface areas of TPI-1@IC and TPI-2@IC were 1053 m^2 g^{-1}, 814 m^2 g^{-1}, respectively, which were higher than those of TPI-1 (809 m^2 g^{-1}) and TPI-2 (796 m^2 g^{-1}) with the same chemical composition. Different from the reaction conducted in sealed vessels, an open crucible was used in a two-step approach where the first trimerization reaction was run at lower temperatures and the next polymerization and crystallization took place in the molten salt.[58] Pre-CTF was prepared in chloroform/TFMSA at 40 °C. In a further study, a molar ratio of 1 : 0.8 of pre-CTF to $ZnCl_2$ was employed to realize CTF-1$_{(open)}$ while traditional CTF-1$_{(sealed)}$ was obtained with a molar ratio of 1 : 1 of monomer to $ZnCl_2$. After 40 h reaction time, the BET surface area of CTF-1$_{(open)}$ was 910 m^2 g^{-1} which was well comparable to that of CTF-1$_{(sealed)}$ (791 m^2 g^{-1}).

2.1.2. TFMS-catalyzed trimerization reaction. Different from the black-colored products obtained *via* the $ZnCl_2$-based

trimerization reaction, the CTFs synthesized under TFMS-catalyzed conditions show fluorescence characteristics which varied with building monomers. And TFMS-based trimerization is usually conducted under mild conditions, which enables the utilization of chemically and thermally unstable monomers. In 2012, Ren et al. synthesized P1–P6 and P1M–P2M via TMFS-catalyzed condensation under room temperature and microwave conditions, respectively.[59] The nitrogen content of P1–P6 and P1M–P6M was closer to the expected values than that of the product obtained from ionothermal $ZnCl_2$-catalyzed synthesis, which means fewer overall defects. Notably, P1–P6 fabricated at room temperature showed an amorphous structure, while P1M, P2M and P4M obtained via MW-assisted methods showed preferred orientation and limited crystallinity. In the MW-assisted reaction, the Brønsted acidic environment along with the increased pressure can facilitate the breaking and bonding of the triazine block at lower temperatures. Therefore, ordered domains can be formed through the thermodynamic function in the overall amorphous network. Moreover, the BET surface area of P2M–P6M was lower than that of P2–P6. Take P6 and P6M as representative examples: P6 was synthesized at room temperature while P6M was synthesized at 110 °C under a MW power output of 300 W, and both have the same backbone. The BET surface area of P6 ($1152 m^2 g^{-1}$) was much higher than that of P6M ($947 m^2 g^{-1}$). Similar results have been observed in other related studies such as in some porous organic cages where lower porosity can be found in more ordered materials.[60] Subsequently, tetraphenylethylene (TPE) based PCTF-8 was also prepared at room temperature by using TFMS as the catalyst.[61] This as-synthesized PCTF-8 exhibited photoluminescence behavior under UV light, while the sample synthesized under the high-temperature $ZnCl_2$-catalyzed conditions did not show apparent emission due to partial carbonization. Interestingly, F-CTF1 and F-CTF3 synthesized by the TFMS-catalyzed method possessed a high proportion of micropores while F-CTF2

synthesized under the same conditions showed no porosity.[62] What is worth mentioning is that porous F-CTF2 could be formed using the same monomer tetra(4-cyanophenyl)ethylene under ionothermal conditions.[63] Similar results could be found where CTF-1 condensed from 1,4-dicyanobenzene under ionothermal condition showed permanent porosity while P1 and P1M which have the same chemical structure as CTF-1 showed no porosity.[39,56,59] There are two possible explanations that lead to the high porosity formed in the $ZnCl_2$ ionothermal reaction: one is the template effect of $ZnCl_2$, and the other is the defects caused by the high temperature. Another modified one-pot solution synthesis of CTFs was presented as an interfacial reaction by Xu and co-workers.[64] This method enabled the easy control of reversibility and the van der Waals epitaxial effect, which was conducive to the growth of a two-dimensional polymer (2DP). Intriguingly, this reaction could be achieved in tens of minutes which was much faster than the abovementioned methods.

Different from liquid-phase reaction conditions, CTFs based on cyclotrimerization of nitriles can be prepared under a TFMS vapor atmosphere at elevated temperature (100 °C) in solid phase synthesis (Fig. 4).[65] Removable templates, silica nanoparticles (SiO_2 NPs), were employed to ensure the ordered and hollow nanostructure of CTFs, and the observation showed that there was no apparent collapse after removing the SiO_2 template, which was irreversible using TFMS solution. Notably, the BET surface areas of the as-prepared CTFs were higher than that obtained from liquid phase synthesis. The authors further synthesized CTF-Th onto mesoporous silica SBA-15, which verified the universality of the method.[66]

Comparing the two trimerization reactions above, the advantages of the TFMS-catalyzed trimerization reaction are obvious: (1) shorter reaction time and lower temperature; (2) avoiding product contamination by extra $ZnCl_2$ catalyst; and (3) eliminating undesired thermal decomposition and side condensation
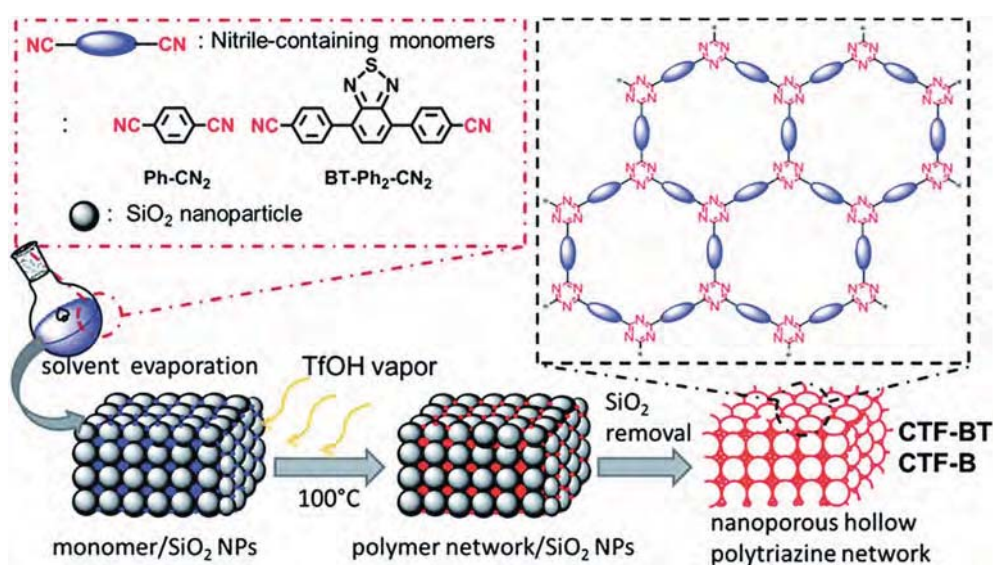

Fig. 4 Scheme of solid phase synthesis and structures of CTF-BT and CTF-B. Reproduced with permission from ref. 65. Copyright 2016, Royal Society of Chemistry.

This journal is © The Royal Society of Chemistry 2019

J. Mater. Chem. A, 2019, 7, 22848–22870 | 22853

reactions such as carbonization and C–H bond cleavage and therefore decreasing framework defects. However, the strong acidic nature of TFMS needs to be taken into account.

2.2. Friedel–Crafts reaction

Cyanuric chloride (CC) with a built-in triazine core is a qualified candidate in the synthesis of CTFs. Accordingly, a series of CTFs were synthesized *via* Friedel–Crafts reaction of CC with aromatic compounds.[67] CC was reacted with benzene (denoted as polymer 2), biphenyl (denoted as polymer 3), and terphenyl (denoted as polymer 4) for 24 h under reflux in dichloromethane with the catalysis of $AlCl_3$, separately. The substitution reaction mainly occurred at the *para*-positions of the aromatic compounds. It was found that the accessible surface area is positively associated with the length of the aromatic linker. Polymer 3 and polymer 4 with increased length of the aromatic linker showed a higher surface area. Similarly, four microporous CTFs based on CC with tri-, dual, and tetra-reactive units of 1,3,5-triphenylbenzene, *trans*-stilbene, and 1,1,2,2-tetraphenylethylene/tetraphenylsilane were obtained *via* an $AlCl_3$-catalyzed Friedel–Crafts reaction.[68,69]

Methanesulfonic acid can also be used as the catalyst of the Friedel–Crafts reaction. Xiong *et al.* and Das *et al.* polymerized triphenylamine with CC using methanesulfonic acid-catalyzed and $AlCl_3$-catalyzed Friedel–Crafts reaction, separately.[70,71] On one hand, methanesulfonic acid as a miscible liquid catalyst enabled the substantial improvement of the reaction efficiency and the products showed fluorescence properties. On the other hand, the strong acid methanesulfonic acid in large excess (14 times excess) requires careful handing. Catalysis by $AlCl_3$ is much milder and the products have a larger surface area.

Recently, an innovative mechanochemical approach was applied to synthesize CTFs *via* the Friedel–Crafts reaction.[72] In this report, carbazole, acting as an electron-rich substrate, was selected to be a model monomer and employed as an activating agent along with CC and $AlCl_3$. With the activating agent in a stoichiometric amount and a bulking agent $ZnCl_2$, a planetary ball mill was used to mill them for 1 h to obtain a porous CTF. Compared to the CTFs obtained in ampoules, the materials prepared under the conditions of ball milling possessed a higher C/N ratio, thus indicating the absence of carbonization. Other monomers such as anthracene and triphenylbenzene were also utilized to prove the generality of this approach.

2.3. Schiff-base reaction

The Schiff-base reaction with a reversible nature enables the formation of a crystalline framework. In addition, the possible utilization of diverse experimental conditions and various molecular precursors extends its feasibility and therefore application in CTF fabrication. Triazine-containing monomers with amino nodes, such as melamine,[73] 1,3,5-tris-(4-aminophenyl)triazine,[74] and 2,4,6-tris(4-aminophenoxy)-1,3,5-triazine,[75] are well-suited for the synthesis of CTFs *via* Schiff-base chemistry (Fig. 5). Mullen and co-workers prepared a series of SNWs *via* the Schiff-base reaction of melamine and
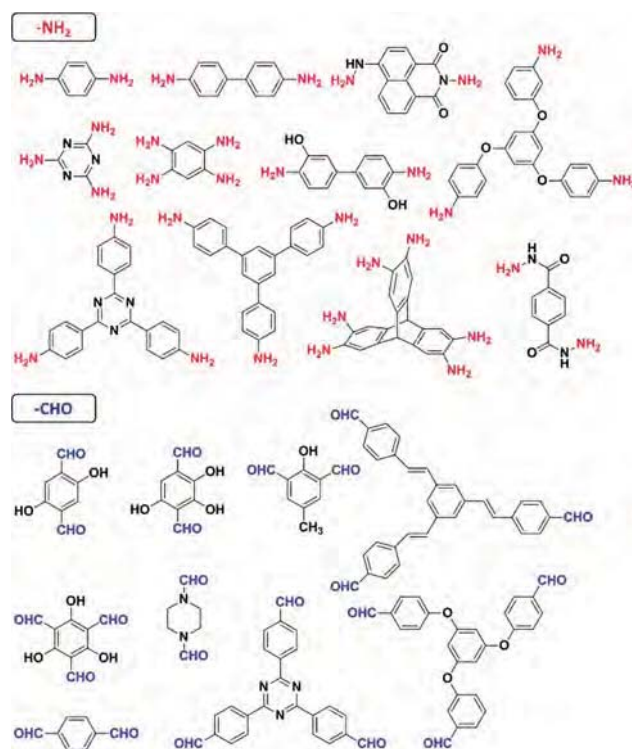
Fig. 5 Building blocks bearing amine and aldehyde units involved in the Schiff-base reaction.

di-/trialdehydes by heating monomers in dimethyl sulfoxide at 180 °C under inert conditions for 72 h.[76] The as-prepared materials showed a high surface area and varied microporosity with different monomers. Moreover, as there is no catalyst used, the products are protected from contamination with inorganic remains. Later, Zhu and co-workers synthesized SNW-1 with the same monomers but different synthesis conditions.[77] The SNW-1 nanoparticles were obtained by the reaction of melamine and terephthalaldehyde under microwave conditions. Compared to SNW-1 prepared under traditional solvothermal conditions for 3 days, the reaction time (6 h) was dramatically reduced and the microporous framework with mesopores was formed *via* the microwave method. In addition, 1,3,5-tris-(4-aminophenyl)triazine was used more than once to condense with aldehyde to obtain CTFs.[78,79] Bhaumik *et al.* developed a triazine-based covalent organic polymer TRITER-1 by the condensation of 1,3,5-tris-(4-aminophenyl)triazine and terephthaldehyde *via* the Schiff-base reaction at a temperature of 150 °C for 12 h in anhydrous dimethylformamide under an inert atmosphere.[80] Then, they further synthesized another CTF TRIPTA by Schiff-base condensation of 1,3,5-tris-(4-aminophenyl)triazine and 1,3,5-triformylphloroglucinol, which involved a reversible condensation and an irreversible keto–enol tautomerization.[81] Specifically, the reversible condensation aims to obtain a highly ordered framework and the keto–enamine formation helps to maintain the high thermal and chemical stability.

Similarly, aldehydes with a triazine core are also regularly used for CTFs.[82–86] Triazine-based benzimidazole-linked

polymers (TBILPs), TBILP-1 and TBILP-2, were prepared by the polymerization of 2,4,6-tris(4-formylphenyl)-1,3,5-triazine (TFPT) with 1,2,4,5-benzenetetraamine tetrachloride (BTA) and 2,3,6,7,14,15-hexaaminotriptycene (HATT), respectively.[87] The BET surface area of TBILP-1 and TBILP-2 was 330 m^2 g^{-1} and 1080 m^2 g^{-1}, respectively. The introduction of the triptycene core enables TBILP-2 to have a high internal molecular free volume and low interpenetrated networks. In addition, Zhou and co-workers constructed a new triazine-based covalent organic polymer (COP-NT) by condensing a naphthalene imide derivative and triazine derivative with a mixture of mesitylene, 1,4-dioxane and glacial acetic acid under the conditions of 120 °C for three days.[85] Interestingly, the as-prepared COP-NT showed amorphous features reflected by the powder X-ray diffraction (PXRD) pattern.

2.4. Nucleophilic substitution reaction

Besides in the Friedel–Crafts reaction, CC with the triazine core is also favorable in nucleophilic substitution reactions. Each chloro group of CC can be substituted via reacting with nucleophiles such as alcohols, thiols and amines, and the number of substitutions can be varied by controlling the temperature and other related factors. Several CTFs were fabricated via the nucleophilic substitution reaction based on CC.[88–90] Zhao et al. prepared a novel triazine-based porous organic framework PAF-6 based on CC, and piperazine acted as a linear linker.[91] The polymerization in a solution mixture of THF and DIPEA was first conducted in an ice-bath for 4 h and then at a temperature of 90 °C. The Fourier transform infrared spectra (FT-IR) of PAF-6 confirmed the substitution of three chlorine atoms. PAF-6 exhibited high stability in common organic solvents such as acetone and DMF and showed a certain degree of crystallinity which was possibly because of the introduction of piperazine and the kinetically controlled nature of the polymerization. Bai et al. chose CC as a center node to react with targeted linker molecules including urea, thiourea and thiosemicarbazide to synthesize a series of novel functional CTFs (denoted as CCU, CCTU and CCTS, respectively).[92] The aromatic C–N stretching modes at 1551 cm^{-1} in the FT-IR spectra indicated the presence of the triazine unit in these as-prepared products. The products showed partial crystallinity while disordered structures in long-range order. Similarly, Pitchumani et al. developed a kind of mesoporous covalent organic polymer (MCOP) based on 4,4′-dihydroxybiphenyl and CC, which showed partial crystallinity and a certain degree of order.[93]

Patel et al. synthesized COP-3 via a conventional nucleophilic aromatic substitution in which 1,3,5-benzenetrithiol reacted with triazine-containing CC, losing the three destabilized chlorides to form an insoluble mass with R–S–R bonded networks.[94] In detail, DIPEA was added to the mixture of 1,3,5-benzenetrithiol and 1,4-dioxane at 15 °C. And CC was dissolved in 1,4-dioxane and then dropwise added to the solution of DIPEA, 1,3,5-benzenetrithiol and 1,4-dioxane with continuous stirring in a N$_2$ environment at 15 °C. The as-prepared product was first stirred at 15 °C for 1 h and then at 25 °C for 2 h before being stirred at 85 °C for 21 h. Similarly, COP-4, COP-5 and COP-6 based on 1,4-benzenedithiol,

biphenyl-4,4′-dithiol, 4,4′-thiobisbenzenethiol were also prepared. The complete substitution of chloride from CC could be observed from the FT-IR spectrum, confirming the formation of sulfur bridged COPs. And COP-3 exhibited the highest BET surface area of about 413 m^2 g^{-1}.

2.5. Condensation reaction of amine with dianhydrides

A series of polyimide-contained CTFs were prepared via the polymerization of melamine and dianhydride monomers in dimethyl sulfoxide at 180 °C under inert conditions for 72 h.[95] The as-prepared polymers were amorphous while the products synthesized by directly heating monomers showed acceptable crystallinities.[96] Similarly, condensation of melamine and perylene-3,4,9,10-tetracarboxylic dianhydride (PTCDA) was achieved using a Lewis acid catalyst (zinc acetate and imidazole complex).[97] The obtained PI-network showed good thermal stability with a uniform ultramicropore size which was less than 6 Å. Recently, pyromellitic dianhydride and 1,3,5-tris-(4-aminophenyl)triazine were polymerized in a mixture of mesitylene, NMP and isoquinoline at a temperature of 160 °C for 5 days.[98] The as-synthesized framework showed good thermal and chemical stability and a BET surface area of 1484 m^2 g^{-1}.

2.6. Other related synthetic methods

A porphyrin-based POP with a triazine skeleton (named TPOP-1) was condensed with 4,4′,4″-(1,3,5-triazine-2,4,6-triyl)tris(oxy)tribenzaldehyde with pyrrole under acid hydrothermal conditions (Fig. 6a).[99] The porous framework of TPOP-1 with a BET specific surface area of 560 m^2 g^{-1} was prepared as follows: first, the strong acid reaction medium enables the protonation of the aromatic aldehyde and then the electrophilic aromatic substitution at the pyrrole occurs, thus generating porphyrin centers with three free –CHO groups per triazine unit and subsequently undergoing further condensation with another pyrrole. The solid-state MAS-NMR and FT-IR spectra confirmed the existence of porphyrin and triazine units in TPOP-1 (Fig. 6b and c). Besides, amorphous TCMPs with a 1,3,5-triazine node were developed via (A3 + B2) or (A3 + B3) Sonogashira–Hagihara cross-coupling reactions by using a 1.5 : 1 molar ratio of ethynyl to bromo functionalities and employing DMF as a solvent.[100] Networks formed by A3 + B3 copolymerization (TCMP-0: 963 m^2 g^{-1}, TNCMP-2: 995 m^2 g^{-1}) had higher surface areas than those obtained from A3 + B2 reactions (TCMP-3: 691 m^2 g^{-1}, TNCMP-5: 494 m^2 g^{-1}). Zhang et al. developed a multifunctional carbazole-based conjugated microporous polymer MFCMP-1 based on 2,4,6-tris(carbazolo)-1,3,5-triazine by FeCl$_3$-promoted oxidative coupling polymerization.[101] The as-prepared MFCMP-1 possessed a large BET surface area of over 840 m^2 g^{-1} with a pore volume of 0.52 cm^3 g^{-1}. And different from other COFs with a crystalline nature, it showed an amorphous nature.

In addition, other methods including Yamamoto coupling reaction and Stille cross-coupling polymerization have also been used to synthesize CTFs. For example, Ni-catalyzed Yamamoto reaction was employed by Cao and co-workers to synthesize a series of COPs based on tris(4-bromophenyl)
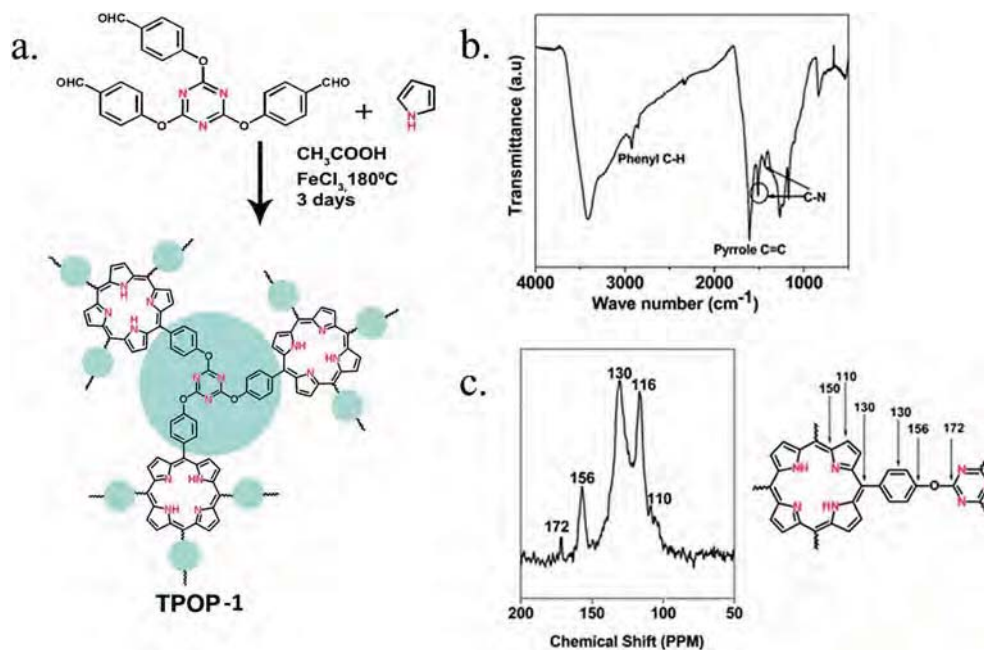
This journal is © The Royal Society of Chemistry 2019

J. Mater. Chem. A, 2019, 7, 22848–22870 | 22855

Fig. 6 (a) Schematic representation of the synthesis of Pd-TPOP-1; (b) FT-IR spectrum of TPOP-1; (c) solid-state MAS-NMR of TPOP-1. Reproduced with permission from ref. 99. Copyright 2014, Royal Society of Chemistry.

amine, 2,4,6-tris-(4-bromo-phenyl)-[1,3,5]triazine, and 1,3,5-tris(4-bromophenyl)benzene.[102] All the COPs possessed a high BET specific surface area and high hydrothermal stability as well as a graphene-like layer texture. Later, they further prepared triazine-containing COP-T with hydrothermal stability by the self-coupling of 2,4,6-tris-(5-bromothiophen-2-yl)-[1,3,5] triazine (TBYT).[103] The characteristic peak at 512 cm^{-1} observed from the FT-IR spectra of COP-T belongs to the C–Br stretching vibration, which indicated complete Br elimination via phenyl–phenyl coupling in the Yamamoto reaction. Gontarczyk and co-workers developed hybrid triazine-boron COFs (BTA-COFs) by a "one-pot" dehydration reaction.[104] Yu and co-workers fabricated PCTF-1 with triazine rings via phosphorus pentoxide catalyzed condensation based on aromatic amides rather than aromatic nitriles.[105] Kim and co-workers synthesized triazine-based covalent organic nanosheets with 2,5-bis(trimethyl-stannyl)thieno-(3,2-b)thiophene and 2,4,6-tris(5-bromothio-phen-2-yl)-1,3,5-triazine (M2) through a Stille cross-coupling reaction.[106]

Recently, a new condensation strategy involving a Schiff base reaction followed by a Michael addition was proposed for the reaction of aldehydes and amidines.[107] CTFs named CTF-HUST-1, CTF-HUST-2, CTF-HUST-3 and CTF-HUST-4 were prepared at relatively low temperature (≤ 120 °C) and ambient pressure which enabled large scale synthesis. Later, the authors improved this strategy to obtain crystalline CTFs by slowing down the nucleation process through in-suit formation of aldehyde monomers by controlled oxidation of alcohol monomers.[108] The results demonstrated that CTF-HUST-C1 achieved using the alcohol oxidation strategy had a better crystalline structure than the previous CTF-HUST-1. Generally, two steps are needed: at first the polymerization reaction occurs at a lower

temperature for aldehyde formation control and then the enhanced polymerization rate is maintained at a higher temperature for improved crystallinity. And to further address the crystallinity issue, the same group developed a controlling feeding rate method to synthesize highly crystalline CTFs.[109] The nucleation process can be controlled by regulating the concentration with the feeding rate in an open system. According to this strategy, CTF-HUST-HC1 and CTF-HUST-HC2 were prepared which possessed a better NO removal rate than amorphous CTF-HUST-1.

3. Characterization of CTFs

Characterization of CTFs is essentially similar to that of COFs, which includes studying atomic connectivity, structural regularity, morphology, and porosity. Powder X-ray diffraction (PXRD) is often used to analyse the structural regularity and the long range ordering.[48] Unfortunately, most CTFs are amorphous, which makes the characterization quite troublesome and reveals limited information about the conformations. The atomic connectivity in CTFs, especially for the formation of linking bonds, is another important parameter for characterization. Solid-state nuclear magnetic resonance (NMR) spectroscopy, as a common but strong technique, has been well applied in other porous materials including zeolites[110] and MOFs,[111] which is undoubtedly useful in characterizing CTFs. Many atoms in the CTFs, e.g. ^{13}C, ^{1}H, ^{17}O, and ^{15}N, possess nuclear spin I, which endows them with NMR signals. For example, in the synthesis of CTF-CSU, NMR such as ^{13}C NMR and ^{1}H NMR is a useful tool to confirm the structure of the corresponding precursors and intermediates.[112] Meanwhile, other characterization methods, such as elemental analysis

22856 | *J. Mater. Chem. A*, 2019, **7**, 22848–22870

This journal is © The Royal Society of Chemistry 2019

(EA), infrared radiation (IR) and ultraviolet visible (UV-vis) spectroscopy, are also feasible, providing additional information on CTFs.[113] And thermogravimetric analysis (TGA), as one of the most accessible methods, can also not be neglected, which can provide first-hand information to investigate the thermal stability of CTFs.[114]

The surface area and porosity of CTF materials are normally assessed by gas (nitrogen or argon) adsorption–desorption measurements. For example, the porosity parameters of Tz-df-CTF materials were obtained by using N_2 adsorption–desorption isotherms measured at 77 K.[115] The BET surface area was determined to be 1550 m^2 g^{-1} for Tz-df-CTF400, 1878 m^2 g^{-1} for Tz-df-CTF500, and 2105 m^2 g^{-1} for Tz-df-CTF600, combining a total pore volume of 0.89, 1.08, and 1.43 cm^3 g^{-1}, respectively. Scanning electron microscopy (SEM), transmission electron microscopy (TEM) and atomic force microscopy (AFM) are often used to probe the morphology, size and crystallinity. A representative example of their use was found in the study of CTF-HUST-HC1.[109] TEM, SEM, and AFM are utilized to analyse the morphology to reach a conclusion that CTF-HUST-HC1 possesses a micrometer-size layered structure and a thickness of 4.7 nm. HR-TEM images further revealed its highly crystalline nature. In addition, X-ray photoelectron spectroscopy (XPS) is helpful to investigate the state of metal ions incorporated into the CTFs.[116]

Besides experimental studies, theoretical computation is an essential and useful auxiliary technique for investigating the structure and function of the frameworks. A majority of theoretical research focuses on the structural modelling of the CTFs, while others figure out the properties and application prediction, such as hydrogen storage capability. Molecular modelling provides important information for the characterization and application of CTFs in a predictive way. For example, in the study of Prof. Zhao, the electronic structure, work function, optical properties, and band edge alignment for monolayer and multilayer CTFs have been investigated by using first-principles calculations.[117]

4. CO$_2$ capture performance of CTFs

The successful structure and property design of CTFs inspired researches to investigate their performance in CO_2 capture. In recent years, studies on the application of CTFs in CO_2 capture have sprung up rapidly. The relevant surface area, pore parameters and CO_2 capacities of CTFs are summarized in Table 1.[118-131] And to further illustrate the advantages and feasibility as well as the current limitations of CTFs for CO_2 capture, their CO_2 capture performance under different conditions is analyzed and discussed.

4.1. CO$_2$ adsorption at low pressures

The CO_2 capture capacity is a significant criterion to judge the CO_2 capture performance of porous materials. The ability of CO_2 adsorption and selectivity at low pressure is very important for the effective separation of CO_2 in the process of post-combustion.[132] In low-pressure adsorption, the capacity performance depends more on the CO_2–sorbent interaction than on the surface area. Generally, CTFs with micropores of less than 1 nm may show more effective CO_2 adsorption due to the molecular size of CO_2 (0.36 nm). For example, PHCTF-4 and PHCTF-6 had a higher BET surface area than PHCTF-1a. And the V_{micro}/V_{total} value of PHCTF-1a, PHCTF-4 and PHCTF-6 was 79%, 58% and 39%, respectively, which indicates the more mesoporous structure of PHCTF-4 and PHCTF-6. The results indicated that the CO_2 adsorption capacities of PHCTF-4 (52.4 cm^3 g^{-1}) and PHCTF-6 (51.9 cm^3 g^{-1}) did not show significant difference from that of PHCTF-1a (51.9 cm^3 g^{-1}), even though they have a higher surface area.[124,133] Therefore, designing uniform or ultra microporous CTFs is an effective means for improving the low-pressure CO_2 adsorption capability. Still, in addition to the comparative micropore volume, a larger surface area certainly can also endow the materials with higher CO_2 adsorption capacity. Moreover, the surface functional groups of the materials have a more significant effect. Compared to CTFs without polar groups on the pore wall, CTFs that have polar groups show more excellent CO_2 capture performance owing to the stronger interaction between CO_2 molecules and polar groups. The surface nature of CTFs plays a more important role at low pressure than the surface area. For example, FCTF-1 and FCTF-1-600 exhibited higher initial isosteric heat values of CO_2 adsorption (Q_{st}) than CTF-1 and CTF-1-600, which indicated that the introduction of C–F bonds indeed enhances their affinity to CO_2 (Fig. 7). Meanwhile, compared with CTF-1, CTF-1-600 possessed a smaller micropore surface area whereas a higher CO_2 adsorption. This may be because the nitrile groups in CTF-1-600 have stronger affinity to CO_2 than the nitrogen in CTF-1.[134] Interestingly, efficient nitrogen doping might result in a higher CO_2 capacity than oxygen doping.[135,136]

4.2. CO$_2$ adsorption at high pressures

The performance of CO_2 adsorption at high pressure is very important for the purification of natural gas or the preparation of adsorbed natural gas (ANG) for future small-sized vehicles.[137,138] Different from the low-pressure adsorption mentioned above, high-pressure adsorption by CTFs is greatly determined by the surface area and pore volume. Usually, the CO_2 capture capacity increases with increasing surface area and pore volume due to the multi-layer adsorption under high pressure. Higher CO_2 adsorption was achieved by MCTP-1 with a higher surface area than MCTP-2 at 300 K and 35 bar, respectively.[139] The CO_2 adsorption capacity of the CTF TRIPTA was tested under the conditions of two different temperatures and up to 5 bar pressure. With the increase of pressure, the amount of adsorbed CO_2 increased and reached a maximum value of 290.8 cm^3 g^{-1} at 273 K and 5 bar pressure. And TRIPTA can adsorb more CO_2 with further increase in pressure, considering that the isotherms did not reach any saturation value even though the rate of CO_2 adsorption was relatively slower in the high pressure region.[81] Similarly, CO_2 adsorption of the polymer TRITER-1 showed the same trend at high pressure and reached a maximum value of 300 cm^3 g^{-1} at 273 K under 5 bar pressure.[80]

This journal is © The Royal Society of Chemistry 2019

J. Mater. Chem. A, 2019, 7, 22848–22870 | 22857

Table 1 Surface area, porosity parameters, and CO_2 adsorption related properties of typical CTFs
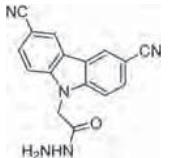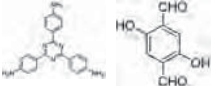
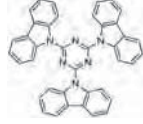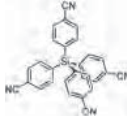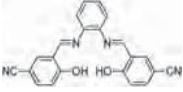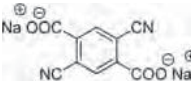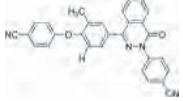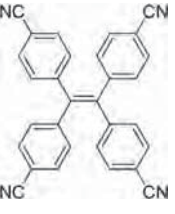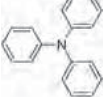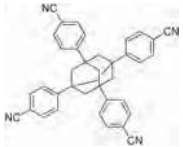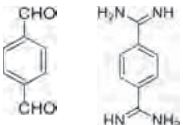| CTFs	Monomers	Surface area [m² g⁻¹]	Pore volume [cm³ g⁻¹]	Pore size [nm]	CO_2 capacities [cm³ g⁻¹] @T^a (K)		Q_{st} [kJ mol⁻¹]	CO_2/N_2 selectivity		Ref.
					Low pressure	High pressure		IAST[b]	Henry	
CTF-CSU37@post		488	0.39		29.0@273					112
TAT-DHBD (1)		750	0.36	2.61, 3.79	30.4@273		27.2			55
TFM-1 (CH₃SO₃H)		738			30.8@273		27.8		48.2	84
PCBZL		341	0.36		32.6@273		39.6	82(148)		143
PAF-16-2		979			42.2@273		30.3			28
Zn@CTF		598.2	0.35	0.53, 1.26	43.9@273		32.5	14.5		130
CTF-CSU41		333	0.78		52.3@273		44.6			112
PHCTF-4		1270	0.79		52.4@273		24.3	35	40	133
PCTF-8		625	0.32		56.0@273		37	24	61	32
NOP-3		894	0.54		56.1@273		33.8	25.6	27.1	49
PCTF-5		1183	0.70		58.1@273		27.0	32.0	17.0	120
CTF-HUST-1		663			63.5@273		30.0			107

Table 1 (*Contd.*)
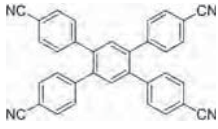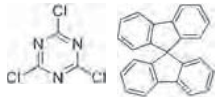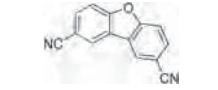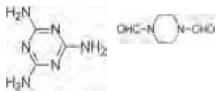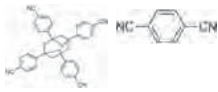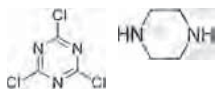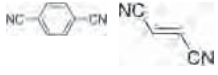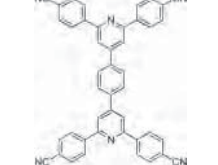
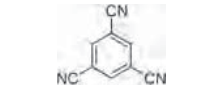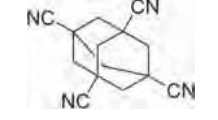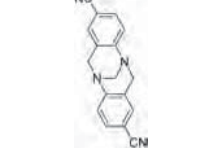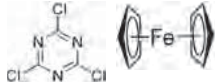| CTFs	Monomers	Surface area [m² g⁻¹]	Pore volume [cm³ g⁻¹]	Pore size [nm]	CO₂ capacities [cm³ g⁻¹] @Tᵃ (K)		Qst [kJ mol⁻¹]	CO₂/N₂ selectivity		Ref.
					Low pressure	High pressure		IASTᵇ	Henry	
F-CTF1		896	0.49		66.1@273		29.7			39
Sbf-TMP@4:2		715	0.41	0.57, 1.0, 1.55	67.7@273		28.6	74		129
cCTF-400		1247	1.04	1.64	67.7@273		43			114
MCTF@500		1510	2.67	0.74	70.8@273		26.3			119
NPTN-2		1558	1.23		71.1@273		37.0	22.0		135
CIN		722			74.6@273		42.2	200(110)	101(92)	125
Ad4L1		1617	0.9		75.5@273		34.3	23		147
CTPP		779	0.77	1.27, 2.96	78.2@273		50	128(84)	88(82)	145
CTF-FUM-500		230	0.12	0.52	78.2@273		58.1		(102.4)	161
CTF-20-400		1458	0.84		78.2@273		22		19	157
CTF-0-9		2011	1.53		79.8@273					31
KPOP-6b		870	0.4	1.22	84.5@273		31.9			52
CTF-TB-3		612	0.35		85.8@273				43.4	123
FMAP-1		875	2.03	2.2	85.9@273		41.6	107	100	142

This journal is © The Royal Society of Chemistry 2019
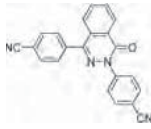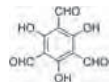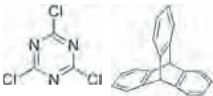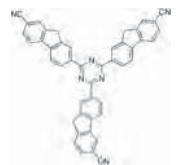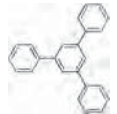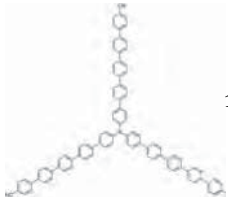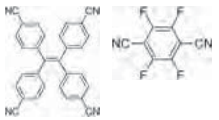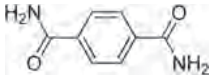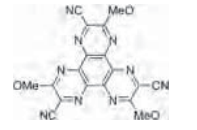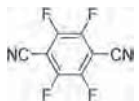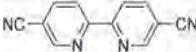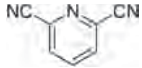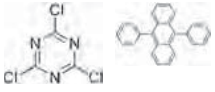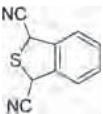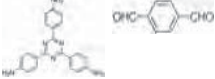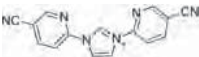
J. Mater. Chem. A, 2019, **7**, 22848–22870 | **22859**

Table 1 (*Contd.*)

CTFs	Monomers	Surface area [m² g⁻¹]	Pore volume [cm³ g⁻¹]	Pore size [nm]	CO₂ capacities [cm³ g⁻¹] @T^a (K)		Q_{st} [kJ mol⁻¹]	CO₂/N₂ selectivity		Ref.
					Low pressure	High pressure		IAST[b]	Henry	
PHCTF1c		1845	1.32	1.3, 5.8	86.9@273		16.0		12	124
TAT-TFP (2)		646	0.44	1.17	87.0@273	290.8@273 [c]	30.0			63
CTF-TPC		1668	0.93	0.59, 0.73, 1.18, 1.48	95.2@273		32	30	20	122
Fl-CTF300		1235	0.67		96.2@273		32.7	23.0	27.0	121
MCTP-1		1452	0.73	1.51	104.0@273		40		(15.4)	92
PCTF-4		1404	0.59	0.54	104.2@273				56	135
MM2		1360	0.67		106.8@273		32	44	23	128
PCTF-1		1200	0.62	1.3	110.2@273		44.5		(46.1)	48
pCTF-1		2034.1	1.04	1.00	110.8@273		30.7			108
HAT-CTF-450/600		1090	0.26		114.6@273		27.1	183	160	126
TBILP-2		1080	0.60	1.10	116.0@273		29.0	(43.0)	(40.0)	62
FCTF-1-600		1535		0.46, 0.59	124.0@273		32.0	19.0		134

Table 1 (Contd.)

CTFs	Monomers	Surface area [m² g⁻¹]	Pore volume [cm³ g⁻¹]	Pore size [nm]	CO$_2$ capacities [cm³ g⁻¹] @T^a (K)		Q_{st} [kJ mol⁻¹]	CO$_2$/N$_2$ selectivity		Ref.
					Low pressure	High pressure		IAST[b]	Henry	
bipy-CTF600		2479	0.98		125.5 @273		34.4	(24)	(37)	141
CTF-py[HT]		3040	1.51		134.2@273		27.1		29	152
caCTF-1-700		2367	0.98		134.9@273		30.6			150
aPCTP-3c		2271	0.95	0.76, 1.33, 2.17, 3.02	144.8@273		35.8		23.7(20.8)	160
Tz-df-CTF600		2106	1.43		170.2@273		20.0	(16.8)	5.7	115
CTF-DCBT		500	0.26		37.8@298		44.2		(112.5)	148
TRITER-1		716	0.32	1.75		300@273[c]	38.1			60
Bpim-CTF500		1556	0.75	1.0–1.6	79.3@288		28	(23.5)		127

[a] Unless otherwise stated, the low-pressure CO$_2$ capacity was measured at 1 bar. [b] Determined from IAST with CO$_2$/N$_2$ (15 : 85 v/v) at 273 K (298 K) and 1 bar. [c] Measured at 5 bar.

4.3. Gas selectivity and breakthrough performance

In addition to the adsorption performance, gas separation is another important factor to assess the application of porous materials in CO$_2$ capture. And CCS related gas separation usually includes CO$_2$/H$_2$ separation, CO$_2$/N$_2$ separation, air (O$_2$/N$_2$), CO$_2$/CO and CO$_2$/CH$_4$ separation. Generally, selectivity is the main t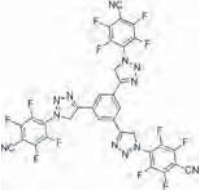ool to weigh up the potential of CTFs in gas separation. In the process of selective adsorption, two indicators need to be considered: adsorption capacity and selectivity. In most cases, single-component adsorption isotherms including Henry's law and ideal adsorbed solution theory (IAST) are used to calculate a material's selectivity. But these single-component adsorption calculations do not always involve all experimental variables as indicated by the name, and thus gas mixture adsorption experiments like breakthrough experiments should also be employed.[140] Lotsch and co-workers presented a series of functional CTFs, containing lutidine, pyrimidine and bipyridine building units, respectively, and calculated the adsorption

equilibrium selectivity of CO$_2$ and N$_2$ from the ratio of the initial slopes in the Henry region and IAST at 298 K.[141] Pym-CTF500 possessed the highest selectivity (Henry: 189, IAST: 502), which outperforms most CTFs measured so far, including FMAP-1 (Henry: 100, IAST: 107),[142] TPI-2@IC (Henry: 69.6, IAST: 151),[57] and PCBZL (IAST: 148).[143] Notably, with the increase of adsorption capacity, the selectivity decreases. This inverse proportionality between adsorption and selectivity is a general trend in porous materials chemistry.[144]

Generally, a breakthrough experiment is a way to evaluate the gas separation performance of CTFs under kinetic flowing gas conditions in real applications, which is more straightforward and reliable than single-component isotherms for the calculation of selectivity. In the breakthrough experiment, the compressed material is placed on an adsorbent bed, and the mixture gas flows through it. A gas chromatograph or mass spectrometer is linked with the gas outlet to analyze the composition of the outgoing gas streams. There are several examples of breakthrough experiments for evaluating the
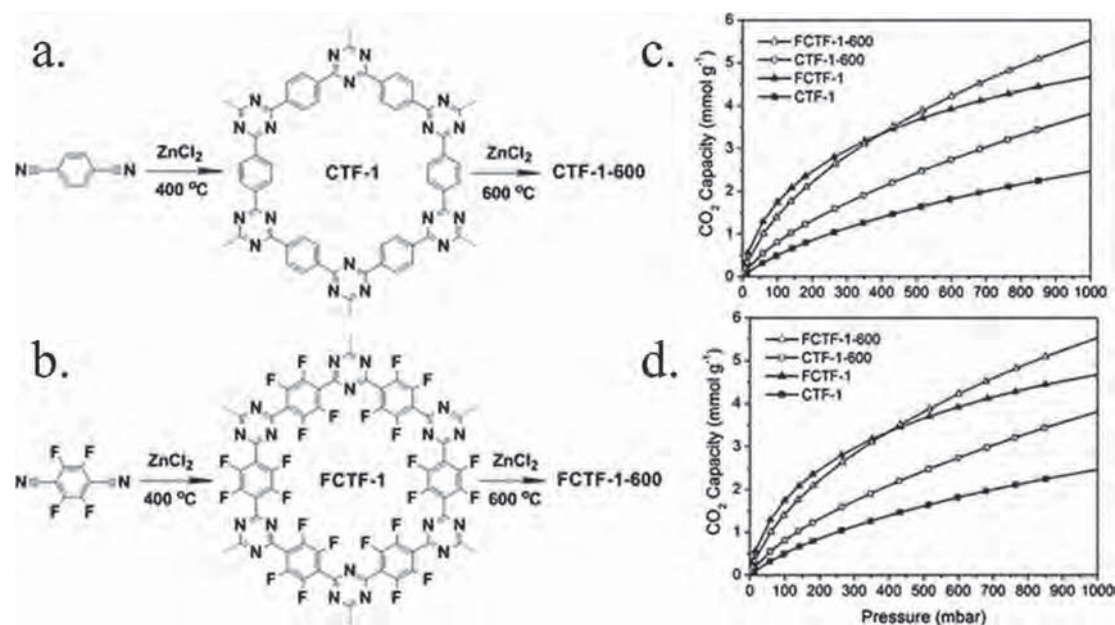
Fig. 7 Reaction schemes and structures of CTFs synthesized through the trimerization of (a) terephthalonitrile and (b) tetra-fluoroterephthalonitrile; (c) CO_2 adsorption isotherms at 273 K; (d) CO_2 adsorption isotherms at 298 K. Reproduced with permission from ref. 134. Copyright 2013, Royal Society of Chemistry.

performance of CO_2 separation in CTFs. Lai and co-workers evaluated the CO_2 separation performance of several CTFs by breakthrough experiments. The experiments were conducted separately, including CTPP using a binary mixture of CO_2/N_2 at 298 K (Fig. 8a and b),[145] TMCOP using steams containing CO_2/N_2 at ambient pressure and temperature (Fig. 8c),[146] and CIN using CO_2/CH_4 or CO_2/N_2 at 298 K (Fig. 8d–f).[147] These CTFs have comparable or better CO_2 capture and separation performance than other porous materials in some cases. Other CTFs such as CTF-DCBT,[148] CTF-FUM and CTF-DCN[116] have also been tested by breakthrough experiments indicating that these CTFs can separate mixed gases of CO_2/N_2 and CO_2/CH_4 completely.

4.4. Heat of CO_2 adsorption

The heat of CO_2 adsorption (Q_{st}) is used to analyze the interaction between CO_2 and the sorbent, which is an important parameter for CO_2 adsorption performance. Usually, the Clausius–Clapeyron equation can be used to calculate the Q_{st} value and first fitting the temperature-dependent isotherm can be used to evaluate for a virial-type expression.[149] For example, the Q_{st} value of CTF-DCN and CTF-FUM was calculated according to the Clausius–Clapeyron equation from CO_2 adsorption isotherms at 298 and 273 K for investigating their binding affinity for CO_2.[116] Q_{st} at zero coverage for CTF-FUM-350, CTF-FUM-400, and CTF-FUM-500 was 58.1, 55.0, and 50.3 kJ mol^{-1}, respectively, which are higher than that of CTF-DCN-400 (30.6 kJ mol^{-1}), CTF-DCN-500 (34.5 kJ mol^{-1}), TRITER-1 (38.1 kJ mol^{-1}),[80] and CTF-1 (39.6 kJ mol^{-1}).[150] The high nitrogen contents and ultramicropores of CTF-FUM might be the reason for its high CO_2 binding affinities. In addition to weighing up

the selectivity adsorption of CTF-FUM for CO_2, the Q_{st} values for N_2 and CH_4 of CTF-FUM were calculated with a result of about 9 and 25 kJ mol^{-1}, respectively. These lower Q_{st} values indicated the weaker interaction between N_2 (CH_4) and CTFs compared with that of CO_2, which indicates a high CO_2/N_2 and CO_2/CH_4 selectivity. Generally, the Q_{st} decreases with the increase of loading. And considering that strong interactions may cause large energy consumption for the regeneration or desorption of the materials, high Q_{st} is not always necessarily good. What is worth mentioning is that Q_{st} values under 50 kJ mol^{-1} indicate that the physical adsorption of CO_2 is conducive to regeneration.[133] The optimal Q_{st} values for separation are 30–50 kJ mol^{-1}.[151] In addition, the Q_{st} can be affected by the framework structure and pore size. CTF-py containing pyridine units possessed a higher Q_{st} value (35.1 kJ mol^{-1}) than CTF-ph (33.2 kJ mol^{-1}) due to the Lewis acid–base interaction between CO_2 and N-basic sites.[152]

4.5. CO_2 capture of CTFs in a humid atmosphere

Considering the inevitable moisture mixed in industry gases and natural gases in practical application, it is necessary to investigate the CO_2 capture performance of CTFs in a humid atmosphere. Understandably, the adsorption of water can cause materials degradation and sometimes the water molecule may compete against CO_2 for adsorption sites. For example, TBILPs with the covalent bonding nature were exceptionally stable in moisture and acids. However, these polymers provided binding sites for water due to the hydrophilic imidazole sites in the framework, which may have influence on CO_2 capture and selectivity.[87] Thus, designing and synthesizing materials with functional polar and basic groups preferring interactions with
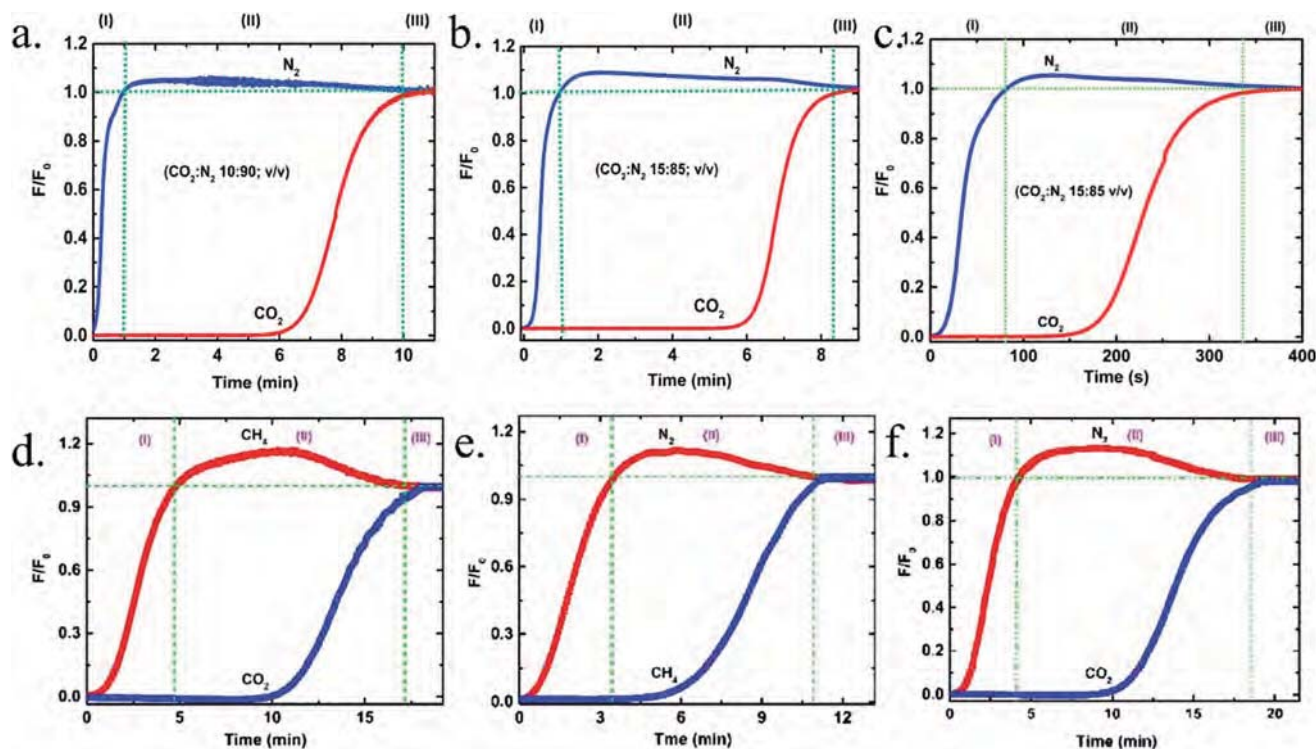
Fig. 8 Column breakthrough experimental results for a CO_2 and N_2 gas mixture at different feed gas compositions after activation with a continuous He flow at 473 K for 12 h. (a) CO_2 : N_2 (10 : 90 v/v) and (b) 15 : 85 measured at 298 K and 1 bar pressure for CTPP materials. Reproduced with permission from ref. 145. Copyright 2016, Elsevier B. V. (c) CO_2 : N_2 (15 : 85 v/v) measured at 298 K and 1 bar pressure for TMCOP materials. Reproduced with permission from ref. 146. Copyright 2018, Elsevier B. V. (d) CO_2 : CH_4 (15 : 85 v/v), (e) CH_4 : N_2 (15 : 85 v/v) and (f) CO_2 : N_2 (15 : 85 v/v) measured at 298 K and 1 bar for CIN materials. Reproduced with permission from ref. 147. Copyright 2017, Elsevier B. V.

CO_2 as well as hydrophobicity would be an effective way. Ramanathan Vaidhyanathan and co-workers designed a triazine-resorcinol based porous polymer HPF-1 functionalized with polar phenolic groups.[153] According to the experimental results, HPF-1 lost only about 5% of the CO_2 adsorption capacity and had a CO_2/N_2 selectivity of 90 : 1 under the conditions of a humid CO_2 stream. Notably, materials with high CO_2 adsorption originating from the nitrogen-rich units may simultaneously increase the affinity to water, which is probably caused by hydrogen bonding.[154]

4.6. Recyclability

Recyclability is an important parameter considering the practicality and economic feasibility of CTFs in large-scale CO_2 capture application. Generally, recyclability can often be investigated by repeated experiments of CO_2 adsorption/desorption cycles and regeneration in the laboratory. It is easy to understand that to be an economically feasible process, an ideal adsorbent must have a large CO_2 adsorption capacity and good selectivity to CO_2. On the other hand, the interaction between CO_2 and adsorbents cannot be too strong, so as to avoid extra drag in the regeneration process. Reproducibility of two CTFs named CTF-FUM and CTF-DCN was investigated by conducting adsorption–desorption cycles at 298 °C.[116] The results demonstrated that the adsorption was reversible and

no obvious loss of activity was observed even after ten cycles, indicating the excellent recyclability of two CTFs without any other heat energy input. Another study showed that the reproducibility of CO_2 adsorption for TPOP-1 was high considering that less than 4.0 wt% decrease in the CO_2 adsorption capacity was observed after five consecutive adsorption–desorption cycles.[155]

5. Strategies for enhancing the CO_2 adsorption ability of CTFs

The inherent characteristics of CTFs, such as various synthetic methods, tailored structure and tunable functionalization, motivate us to investigate their CO_2 adsorption related quality. Generally, high adsorption capacity and selectivity are two primary considerations for the effective adsorption of materials. Considering the CO_2 adsorption capacity and selectivity of materials, there are two factors needed to be emphasized: (1) compared to the micropores and mesopores, narrow ultra-micropores (<1 nm) are preferred in CO_2 adsorption because they could enhance CO_2 molecule occupancy in consideration of the CO_2 thermodynamic size; (2) suitable bonding energy is needed for high adsorption and desorption performance. As for the former, controlling the pore size and surface area is of great importance. As for the latter, introducing polar functional units

onto the pore surface *via* pre- and post-modification could be one of the common and effective strategies. In this section, several strategies including pore size and surface area control, pore wall functionalization and technical means of optimization associated with adsorption capacity and selectivity are given for enhancing the CO_2 adsorption ability of CTFs.

5.1. Controlling the pore size and surface area

Usually, the pore size and surface area are significant for the performance of adsorbent materials. The size dependent molecular sieve effect has been studied extensively in porous materials, and the kinetic separation of porous materials is also correlated with the adsorbent's pore size and surface area.[156] It is worth mentioning how to achieve equilibrium: the pore size should be small enough to interdict undesired gas while large enough to allow passage of the targeted molecule. CTFs with easily controllable design and synthesis have advantages over traditional zeolites and other similar molecular sieves in regulating the surface area and pore size for gas adsorption and separation.

As mentioned above, generally, the CO_2 capacity depends more on the surface area and pore volume under high pressure. However, there are a few exceptions, such as CTF-BI-10 having a higher surface area but lower CO_2 adsorption compared to CTF-BI-4.[47] The thermal transition hardsphere diameters of the CO_2 molecule is 3.6 Å. A pore size close to the diameter is preferred for CO_2 adsorption. Reaction methods and conditions are of great importance with respect to the pore size and surface area of CTFs. Different reaction conditions including temperature and the amount of catalyst lead to different pore size distributions of CTFs even with the same starting monomer, thus resulting in apparent distinction in CO_2 uptake capacities. As demonstrated by Cooper and co-workers, higher surface areas were obtained through the room temperature method than with the microwave-assisted method.[59] Similarly, in the ionothermal reaction, the amount of monomers and temperature have considerable influence on the porosity and structural characteristics. In a particularly study, upon increasing the reaction temperature from 400 to 500 °C and keeping other conditions the same, the as-prepared CTFs exhibited a higher surface area with a higher CO_2 adsorption capacity.[157] As for the Friedel–Crafts reaction, the pore properties of the products are strongly dependent on the degree of polymerization that is mainly influenced by the reaction mixture concentrations.[70] Specifically, a high system concentration is more favourable in a way to enhance the pore parameters in the concentration range investigated. Thus, the porous characteristics of the samples can be easily controlled by changing the reaction concentration. In addition, chemical activation of materials is another promising strategy to obtain sorbents with a high surface area. Using KOH as the activating reagent to transform CTFs into active carbons with a high surface area is very promising for CO_2 capture.[158,159] For example, microporous CTF-1 was activated with KOH at 700 °C to produce chemically activated CTF-1 (denoted as caCTF-1-700). Generally, KOH is entirely consumed when heating up to 700 °C. The obtained

caCTF-1-700 remarkably possessed deep pores with a higher surface area of 2367 m^2 g^{-1}, thus greatly enhancing the CO_2 adsorption capacities up to 134.9 cm^3 g^{-1} at 1 bar and 273 K (Fig. 9).[150] Likewise, KOH-activated porous materials aPCTP-3c with narrow micropore size distributions possessed a higher surface area (2271 m^2 g^{-1}) and larger micro/total pore volumes (0.87/0.95 cm^3 g^{-1}) than those of pristine porous materials prepared without activation and aPCTP-3c possessed a higher CO_2 adsorption capacity of 144.8 cm^3 g^{-1} at 273 K and 1 bar.[160]

Ren *et al.* demonstrated that polymers originating from more highly branched monomers exhibited a higher surface area.[59] However, Gu *et al.* prepared four triphenylamine-based CTFs (PCTF-1 to PCTF-4).[154] The negative correlation between the BET surface area of PCTFs and branched arms revealed that higher density but lower surface area materials might be obtained from monomers with longer branches. As demonstrated by the authors, compared with PCTF-2, PCTF-4 just changed the middle benzene of the branches to benzothiadiazole; however, its BET specific surface area value and CO_2 adsorption capacity were the highest among the PCTFs. Besides, shortening and widening the size of the monomer is another strategy to construct CTFs with ultramicropores. Zhong and co-workers synthesized CTF-FUM with a short monomer fumaronitrile and CTF-DCN with a wide monomer 1,4-dicyanonaphthalene, respectively. As a result, an ultramicroporous nature was found in CTF-FUM (5.2 Å) and CTF-DCN (5.4 Å), thus endowing them with remarkable adsorption capacity and selectivity for CO_2 over N_2 and CH_4.[161]

In addition to reaction methods and conditions, the size and structural features of building blocks can also affect the pore size. For example, CTF-0 with three functional groups of the 1,3,5-tricyanobenzene monomer has a smaller pore size than CTF-1, while CTF-2 has a bigger pore size than CTF-1 due to its longer monomer (2,6-dicyanonaphthalene). The pore size of the resulting CTFs would vary with the functional groups on building blocks or the length of the building blocks.[162,163] It is obvious that an increase in the BET surface area and micropore ratio in the CTF system can increase the CO_2 capture ability. In the study of Jürgen Senker, functional groups including triazines, imides, ethers, sulfones, and carbonyls had been employed to construct triazine-based polymers.[164] The results demonstrated that microporous TPI-1 with pore volumes of 0.44 cm^3 has the highest CO_2 uptake. Another study has revealed the relationship between CO_2 capture capacity and the building blocks' arm length. A series of CTFs were obtained from triphenylamine and monomers with varied branched arm lengths.[154] The as-prepared CTFs showed that the CO_2 uptake decreased with increase in the arm length. In addition, a twisted and noncoplanar topology moiety is another choice to improve the porosity of CTFs. Phthalazinone structure-based CTFs had been designed with a high BET area of 1845 m^2 g^{-1} and a CO_2 uptake capacity of up to 86.9 cm^3 g^{-1}.[124]

5.2. Functionalization of the pore wall

CO_2 is a highly quadrupolar gas while the competitive sorbates commonly related to CO_2 capture such as H_2, N_2, and CH_4 are
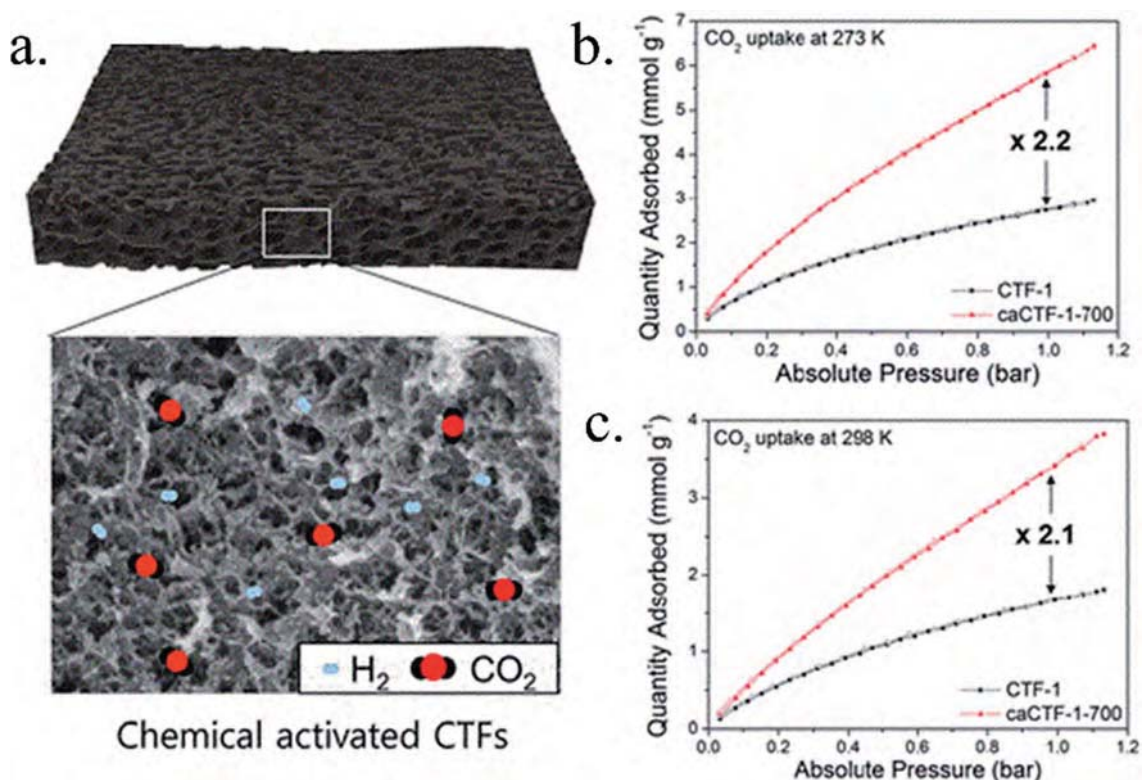
Fig. 9 (a) Schematic diagram of chemical activation CTFs; CO_2 adsorption–desorption isotherms measured at 273 K (b) and 298 K (c) for CTF-1 and caCTF-1-700. Reproduced with permission from ref. 150. Copyright 2017, American Chemical Society.

weakly polar or even non-polar. This indicates that the interactions between these gases and materials are different which can be used to modify the pore surface characteristics of CTFs to enhance the adsorption and separation performance. Generally, the surface characteristics of CTFs can be adjusted by pre-design of building blocks and functional site doping as well as post-modification of existing CTFs.

Locating open active metal sites on the pore walls of CTF provides an approach for enhancing adsorption of quadrupolar gases including CO_2, and separation of non-polar gases including CH_4 and N_2. Liu *et al.* fabricated a class of metal functionalized CTFs polymerized by metalloporphyrin.[119] An improvement of the CO_2 adsorption capacity was observed due to the activated sites on the pore wall which increase the interaction between materials and CO_2. This enhanced adsorption depending on the open metal sites has also been favored in FMAPs. Wang *et al.* constructed iron-decorated microporous aromatic polymers, FMAPs, based on ferrocene and *s*-triazine monomers through Friedel–Crafts reaction.[142] FMAP-1 with a moderate BET surface area showed higher CO_2 adsorption capability and more excellent IAST CO_2/N_2 selectivity than ferrocene-free analogues.

Targeted introduction of functional groups with strong CO_2 affinity into the pores of CTFs is another effective way to enhance the CO_2 adsorption capacity and selectivity. Zhao *et al.* designed a perfluorinated CTF (named as FCTF-1) for selective CO_2 capture.[134] Thermodynamically, the electrostatic interactions between the strongly polar C–F bonds and CO_2 molecules

enhanced CO_2 adsorption, especially at low pressures. Benzimidazole with secondary amine and triazine groups shows CO_2-philic features. CTF-BIs condensed from benzimidazole containing monomers exhibited enhanced CO_2 adsorption capability.[61] Remarkably, CTF-BI-4 and CTF-BI-11 showed higher CO_2 adsorption than CTF-0 derived from TCB,[50] TPI-1–7 containing imide group[164] and many others.[123,124] Another representative study conducted by Liu and co-workers showed that nitrogen- and oxygen-rich phthalazinone structure-based CTFs, PHCTFs, had strong CO_2 affinity and thereby marked CO_2 adsorption capacity.[124] The high electric field on the surface of the framework created by the N, O and S atoms in PHCTFs leads to a remarkable affinity with quadrupolar CO_2 molecules. Especially, efficient oxygen doping is conducive to enhance the CO_2 adsorption under high-pressure conditions, while nitrogen doping tends to achieve higher CO_2 adsorption at relatively low pressure.[56]

Similar to the porous organic polymer scaffolds, charged CTFs have been confirmed to have higher CO_2 adsorption and selectivity than neutral CTFs. Buyukcakir *et al.* reported the first charged CTFs, cCTFs, by an ionothermal reaction based on the monomer cyanophenyl substituted viologen dication.[114] The results revealed that the CO_2 adsorption capacities of cCTFs were higher than those of previously reported CTFs with similar nitrogen contents and surface areas. Indeed, cCTFs with charge centers enabled extra electrostatic interaction with CO_2 molecules and thereby possessed unconventionally high affinity of

This journal is © The Royal Society of Chemistry 2019

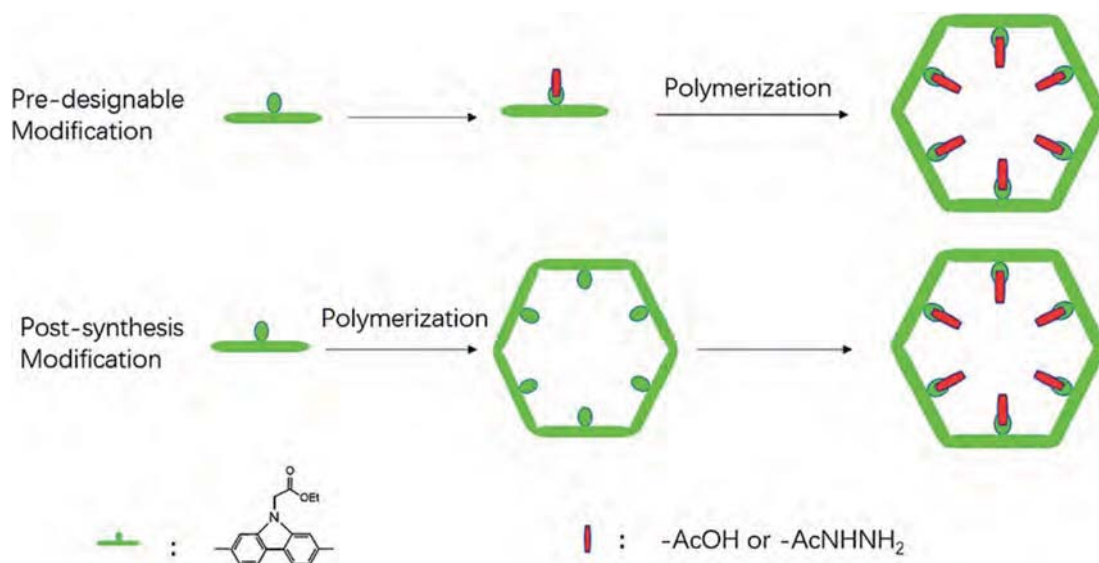*J. Mater. Chem. A*, 2019, **7**, 22848–22870 | **22865**

Fig. 10 Schematic representation of pre-designable and post-synthesis strategies. Reproduced with permission from ref. 165. Copyright 2017, Royal Society of Chemistry.

CO_2, thus leading to a prominently higher CO_2 adsorption capacity than their neutral counterparts.

Yu and co-workers compared the two conventional modification ways, including pre-designable and post-synthesis modification. The incorporating of functional units onto the pore wall was well-controlled by the anchor of acetohydrazides, ethyl ester or acetic acid for highly efficient CO_2 capture (Fig. 10).[165] Two CTFs, CTF-CSU36@pre and CTF-CSU37@pre, were constructed by pre-designed appending of acetic acid or acetohydrazide on the wall. In contrast, post synthesis modification could be achieved by simply hydrolysis or hydrazide reaction of a carbazole-bridged triazine framework with pendant ethyl ester (CTF-CSU20) to obtain CTFs with the surfaces anchored with acetic acid (CTF-CSU36@post) or acetohydrazide groups (CTF-CSU37@post). According to the results, CTF-CSU37@post exhibited the highest CO_2 adsorption of 29 cm^3 g^{-1} at 273 K, which originated from the vital function of acid–base interactions. It is worth mentioning that much higher CO_2 adsorption capacities were achieved in the post-modified samples compared to the pre-designed ones, mainly resulting from the higher pore volume and higher content of appended functionalities of CTF-CSU36@post and CTF-CSU37@post. The oxygen-rich or nitrogen-rich porous frameworks could indeed improve the host–guest interactions due to the enhanced dipole–quadrupole interaction.

5.3. Other technical means

Besides pore size and surface area control and pore wall functionalization, other technical means also can be employed and optimized to improve the CO_2 adsorption and separation capability in CTFs. With respect to the performance of CTF materials in CO_2 capture, the following can be utilized: (1) adjusting the morphological structure and dimensionality of CTFs, such as 3D architectures developed in high-pressure CO_2 adsorption; (2) incorporating CTFs with other materials is also a powerful way to fabricate composites with new properties surpassing those of independent units considering the synergetic effect and thus enhancing the performance; (3) generally, CTFs with different structures possess different CO_2 capture performances. It is necessary to select adsorption and separation methods according to the materials to optimize performance.

6. Conclusions

CO_2 capture has gained extensive attention in both science and technology fields. Obviously, the performance of capture materials is the vital factor for any technology in CO_2 capture. CTFs, as a kind of newly emerging porous material, having the advantages of simple and easily available monomers, easy design and synthesis, and tailored functionalization, show potential for CO_2 capture. Although there have been a variety of synthesized and characterized CTFs that are used as CO_2 capture materials, insufficient development for real-application is still their shortage. Great efforts are essential to solve several critical issues which will impede the development of CTFs for CO_2 capture if they are not addressed.

(1) Only a few crystalline CTFs have been reported. In most cases, the amorphous properties of CTFs cause poor accessibility of binding sites, and therefore fewer binding sites interact with CO_2 molecules in actual operation than that from theoretical calculations. Moreover, it is hard to characterize the amorphous CTFs even by PXRD, which impedes the investigation of the structure of CTFs and thereby hampers the research of the CO_2 capture mechanism. In addition, CTFs are usually prepared in small quantities in laboratories. It can be difficult to scale up in production. Without a workable process for scaling up, CTFs will simply remain as niche materials with little value

for large processing, including carbon capture. Thus, new synthetic methods are still needed.

(2) Compared to experimental studies, computational studies such as molecular simulations and quantum calculations in this field need to be further developed. Clearly, computational studies can be utilized to find useful materials and evaluate the relationships between structure and function, thus providing guidance for the design and optimization of new CTF samples. In CO_2 capture studies, computational studies help decipher the potential of CTFs for CO_2 capture, confirming the experimental results, digging deep into the effects of structural changes, the role of pore size, and the molecular interaction and transport mechanism. In this sense, combining computational studies with experimental efforts is greatly advantageous in the improvement of CTFs for CO_2 capture, which may save both money and time.

(3) To date, the investigations on CTF materials' tolerance to water are limited. In practical CO_2 capture, including pre-combustion capture and post-combustion capture, the gas streams always contain water and it is energy-consuming and even unrealistic to add an extra process for water removal before separation. Thus, materials with excellent water-resistance are preferred in CO_2 capture. Addressing this issue should focus on studies not only about the physical adsorption of water into the pores of CTFs but also about the chemical adsorption of water on the active sites including the open metal center. In addition, very little data on the influence of acid gases during CO_2 adsorption in CTFs have been reported, which also needs to be paid more attention in future studies. And it is clear that the measurement of multi-component adsorption is more practical with respect to real application.

(4) In practical application, it is of great importance to evaluate the reversibility of the CO_2 capture materials, especially at ambient temperature and vacuum cycles, for energy-saving. However, comprehensive studies of reversibility are limited. It is challenging that the reversibility of the CO_2 adsorbents is good while the O_{st} of the adsorbents is 50 kJ mol^{-1} or more. In some cases, the accumulated O_{st} of the entire adsorption process seems to be very high which indicates the difficulty for regeneration. But considering each individual adsorption process, adsorption taking place at different sites may still be reversible and desorption is possible in a sequential program.

Conflicts of interest

There are no conflicts to declare.

Acknowledgements

Notes and references

1 https://www.climate.gov/.

2 D. M. Reiner, *Nat. Energy*, 2016, **1**, 15011.

3 G. Kupgan, L. J. Abbott, K. E. Hart and C. M. Colina, *Chem. Rev.*, 2018, **118**, 5488–5538.

4 J. D. Figueroa, T. Fout, S. Plasynski, H. McIlvried and R. D. Srivastava, *Int. J. Greenhouse Gas Control*, 2008, **2**, 9–20.

5 A. J. Alvaro, I. L. Paniagua, C. G. Fernandez, J. R. Martin and R. N. Carlier, *Energy Convers. Manage.*, 2015, **104**, 170–179.

6 L. K. G. Bhatta, S. Subramanyam, M. D. Chengala, S. Olivera and K. Venkatesh, *J. Cleaner Prod.*, 2015, **103**, 171–196.

7 J. Wilcox, R. Haghpanah, E. C. Rupp, J. J. He and K. Lee, *Annu. Rev. Chem. Biomol. Eng.*, 2014, **5**, 479–505.

8 R. S. Haszeldine, *Science*, 2009, **325**, 1647–1652.

9 S. Nanda, S. N. Reddy, S. K. Mitra and J. A. Kozinski, *Energy Sci. Eng.*, 2016, **4**, 99–122.

10 Y. Yang, C. Zhang, C. Lai, G. M. Zeng, D. L. Huang, M. Cheng, J. J. Wang, F. Chen, C. Y. Zhou and W. P. Xiong, *Adv. Colloid Interface Sci.*, 2018, **254**, 76–93.

11 L. H. Zhang, J. C. Zhang, G. M. Zeng, H. R. Dong, Y. N. Chen, C. Huang, Y. Zhu, R. Xu, Y. J. Cheng, K. J. Hou, W. C. Cao and W. Fang, *Bioresour. Technol.*, 2018, **261**, 10–18.

12 R. Stanger, T. Wall, R. Sporl, M. Paneru, S. Grathwohl, M. Weidmann, G. Schefflmecht, D. McDonald, K. Myohanen, J. Ritvanen, S. Rahiala, T. Hyppanen, J. Mletzko, A. Kather and S. Santos, *Int. J. Greenhouse Gas Control*, 2015, **40**, 55–125.

13 M. Bui, C. S. Adjiman, A. Bardow, E. J. Anthony, A. Boston, S. Brown, P. S. Fennell, S. Fuss, A. Galindo, L. A. Hackett, J. P. Hallett, H. J. Herzog, G. Jackson, J. Kemper, S. Krevor, G. C. Maitland, M. Matuszewski, I. S. Metcalfe, C. Petit, G. Puxty, J. Reimer, D. M. Reiner, E. S. Rubin, S. A. Scott, N. Shah, B. Smit, J. P. M. Trusler, P. Webley, J. Wilcox and N. Mac Dowell, *Energy Environ. Sci.*, 2018, **11**, 1062–1176.

14 M. T. Ho, G. W. Allinson and D. E. Wiley, *Ind. Eng. Chem. Res.*, 2008, **47**, 4883–4890.

15 S. J. Chen, M. Zhu, Y. Fu, Y. X. Huang, Z. C. Tao and W. L. Li, *Appl. Energy*, 2017, **191**, 87–98.

16 N. T. T. Nguyen, H. Furukawa, F. Gandara, H. T. Nguyen, K. E. Cordova and O. M. Yaghi, *Angew. Chem., Int. Ed.*, 2014, **53**, 10645–10648.

17 G. Sethia and A. Sayari, *Carbon*, 2015, **93**, 68–80.

18 A. E. Creamer and B. Gao, *Environ. Sci. Technol.*, 2016, **50**, 7276–7289.

19 G. Singh, K. S. Lakhi, S. Sil, S. V. Bhosale, I. Kim, K. Albahily and A. Vinu, *Carbon*, 2019, **148**, 164–186.

This journal is © The Royal Society of Chemistry 2019

J. Mater. Chem. A, 2019, **7**, 22848–22870 | **22867**

20 D. Saha and M. J. Kienbaum, *Microporous Mesoporous Mater.*, 2019, **287**, 29–55.

21 S. Chaemchuen, N. A. Kabir, K. Zhou and F. Verpoort, *Chem. Soc. Rev.*, 2013, **42**, 9304–9332.

22 M. L. Ding, R. W. Flaig, H. L. Jiang and O. M. Yaghi, *Chem. Soc. Rev.*, 2019, **48**, 2783–2828.

23 Z. Hu, Y. Wang, B. B. Shah and D. Zhao, *Adv. Sustainable Syst.*, 2019, **3**, 1800080.

24 A. A. Olajire, *Renewable Sustainable Energy Rev.*, 2018, **92**, 570–607.

25 O. Cheung and N. Hedin, *RSC Adv.*, 2014, **4**, 14480–14494.

26 D. Bonenfant, M. Kharoune, P. Niquette, M. Mimeault and R. Hausler, *Sci. Technol. Adv. Mater.*, 2008, **9**, 013007.

27 M. Sevilla and A. B. Fuertes, *Energy Environ. Sci.*, 2011, **4**, 1765–1771.

28 J. Wei, D. D. Zhou, Z. K. Sun, Y. H. Deng, Y. Y. Xia and D. Y. Zhao, *Adv. Funct. Mater.*, 2013, **23**, 2322–2328.

29 K. He, G. Q. Chen, G. M. Zeng, A. W. Chen, Z. Z. Huang, J. B. Shi, T. T. Huang, M. Peng and L. Hu, *Appl. Catal., B*, 2018, **228**, 19–28.

30 Z. J. Lin, J. Lu, M. C. Hong and R. Cao, *Chem. Soc. Rev.*, 2014, **43**, 5867–5895.

31 A. Schneemann, V. Bon, I. Schwedler, I. Senkovska, S. Kaskel and R. A. Fischer, *Chem. Soc. Rev.*, 2014, **43**, 6062–6096.

32 M. L. Foo, R. Matsuda, Y. Hijikata, R. Krishna, H. Sato, S. Horike, A. Hori, J. G. Duan, Y. Sato, Y. Kubota, M. Takata and S. Kitagawa, *J. Am. Chem. Soc.*, 2016, **138**, 3022–3030.

33 S. Krause, V. Bon, I. Senkovska, U. Stoeck, D. Wallacher, D. M. Tobbens, S. Zander, R. S. Pillai, G. Maurin, F. X. Coudert and S. Kaskel, *Nature*, 2016, **532**, 348–352.

34 K. Sumida, D. L. Rogow, J. A. Mason, T. M. McDonald, E. D. Bloch, Z. R. Herm, T. H. Bae and J. R. Long, *Chem. Rev.*, 2012, **112**, 724–781.

35 K. Gedrich, I. Senkovska, N. Klein, U. Stoeck, A. Henschel, M. R. Lohe, I. A. Baburin, U. Mueller and S. Kaskel, *Angew. Chem., Int. Ed.*, 2010, **49**, 8489–8492.

36 J. M. Yu and P. B. Balbuena, *J. Phys. Chem. C*, 2013, **117**, 3383–3388.

37 Y. Yang, Z. T. Zeng, C. Zhang, D. L. Huang, G. M. Zeng, R. Xiao, C. Lai, C. Y. Zhou, H. Guo, W. J. Xue, M. Cheng, W. J. Wang and J. J. Wang, *Chem. Eng. J.*, 2018, **349**, 808–821.

38 H. Wang, Z. T. Zeng, P. Xu, L. S. Li, G. M. Zeng, R. Xiao, Z. Y. Tang, D. L. Huang, L. Tang, C. Lai, D. N. Jiang, Y. Liu, H. Yi, L. Qin, S. J. Ye, X. Y. Ren and W. W. Tang, *Chem. Soc. Rev.*, 2019, **48**, 488–516.

39 P. Kuhn, M. Antonietti and A. Thomas, *Angew. Chem., Int. Ed.*, 2008, **47**, 3450–3453.

40 P. Puthiaraj, Y. R. Lee, S. Q. Zhang and W. S. Ahn, *J. Mater. Chem. A*, 2016, **4**, 16288–16311.

41 Y. Zhang and S. B. Jin, *Polymers*, 2019, **11**, 31.

42 M. Y. Liu, L. P. Guo, S. B. Jin and B. E. Tan, *J. Mater. Chem. A*, 2019, **7**, 5153–5172.

43 S. J. Ren, D. L. Zeng, H. L. Zhong, Y. C. Wang, S. X. Qian and Q. A. Fang, *J. Phys. Chem. B*, 2010, **114**, 10374–10383.

44 A. Ranganathan, B. C. Heisen, I. Dix and F. Meyer, *Chem. Commun.*, 2007, 3637–3639.

45 P. Kuhn, A. Forget, J. Hartmann, A. Thomas and M. Antonietti, *Adv. Mater.*, 2009, **21**, 897–901.

46 W. Wang, H. Ren, F. X. Sun, K. Cai, H. P. Ma, J. S. Du, H. J. Zhao and G. S. Zhu, *Dalton Trans.*, 2012, **41**, 3933–3936.

47 L. M. Tao, F. Niu, C. Wang, J. G. Liu, T. M. Wang and Q. H. Wang, *J. Mater. Chem. A*, 2016, **4**, 11812–11820.

48 L. Zhao, S. Shi, M. Liu, G. Z. Zhu, M. Wang, W. Q. Du, J. Gao and J. Xu, *Green Chem.*, 2018, **20**, 1270–1279.

49 M. J. Bojdys, J. Jeromenok, A. Thomas and M. Antonietti, *Adv. Mater.*, 2010, **22**, 2202–2205.

50 P. Katekomol, J. Roeser, M. Bojdys, J. Weber and A. Thomas, *Chem. Mater.*, 2013, **25**, 1542–1548.

51 P. Kuhn, A. Forget, D. S. Su, A. Thomas and M. Antonietti, *J. Am. Chem. Soc.*, 2008, **130**, 13333–13337.

52 J. T. Jia, Z. J. Chen, Y. Belmabkhout, K. Adil, P. M. Bhatt, V. A. Solovyeva, O. Shekhah and M. Eddaoudi, *J. Mater. Chem. A*, 2018, **6**, 15564–15568.

53 W. Zhang, C. Li, Y. P. Yuan, L. G. Qiu, A. J. Xie, Y. H. Shen and J. F. Zhu, *J. Mater. Chem.*, 2010, **20**, 6413–6415.

54 W. Zhang, F. Liang, C. Li, L. G. Qiu, Y. P. Yuan, F. M. Peng, X. Jiang, A. J. Xie, Y. H. Shen and J. F. Zhu, *J. Hazard. Mater.*, 2011, **186**, 984–990.

55 Y. H. Xiong, Y. M. Qin, L. J. Su and F. G. Ye, *Chem.–Eur. J.*, 2017, **23**, 11037–11045.

56 S. F. Wu, Y. Liu, G. P. Yu, J. G. Guan, C. Y. Pan, Y. Du, X. Xiong and Z. G. Wang, *Macromolecules*, 2014, **47**, 2875–2882.

57 S. Wu, S. Gu, A. Zhang, G. Yu, Z. Wang, J. Jian and C. Pan, *J. Mater. Chem. A*, 2015, **3**, 878–885.

58 S. Kuecken, J. Schmidt, L. J. Zhi and A. Thomas, *J. Mater. Chem. A*, 2015, **3**, 24422–24427.

59 S. J. Ren, M. J. Bojdys, R. Dawson, A. Laybourn, Y. Z. Khimyak, D. J. Adams and A. I. Cooper, *Adv. Mater.*, 2012, **24**, 2357–2361.

60 T. Hasell, S. Y. Chong, K. E. Jelfs, D. J. Adams and A. I. Cooper, *J. Am. Chem. Soc.*, 2012, **134**, 588–598.

61 A. Bhunia, D. Esquivel, S. Dey, R. Fernandez-Teran, Y. Goto, S. Inagaki, P. Van der Voort and C. Janiak, *J. Mater. Chem. A*, 2016, **4**, 13450–13457.

62 X. Y. Wang, C. Zhang, Y. Zhao, S. J. Ren and J. X. Jiang, *Macromol. Rapid Commun.*, 2016, **37**, 323–329.

63 A. Bhunia, V. Vasylyeva and C. Janiak, *Chem. Commun.*, 2013, **49**, 3961–3963.

64 J. J. Liu, W. Zan, K. Li, Y. Yang, F. X. Bu and Y. X. Xu, *J. Am. Chem. Soc.*, 2017, **139**, 11666–11669.

65 W. Huang, Z. J. Wang, B. C. Ma, S. Ghasimi, D. Gehrig, F. Laquai, K. Landfester and K. A. I. Zhang, *J. Mater. Chem. A*, 2016, **4**, 7555–7559.

66 W. Huang, B. C. Ma, H. Lu, R. Li, L. Wang, K. Landfester and K. A. I. Zhang, *ACS Catal.*, 2017, **7**, 5438–5442.

67 H. Lim, M. C. Cha and J. Y. Chang, *Macromol. Chem. Phys.*, 2012, **213**, 1385–1390.

68 P. Puthiaraj, S. M. Cho, Y. R. Lee and W. S. Ahn, *J. Mater. Chem. A*, 2015, **3**, 6792–6797.

22868 | *J. Mater. Chem. A*, 2019, **7**, 22848–22870

This journal is © The Royal Society of Chemistry 2019

69 P. Puthiaraj, S. S. Kim and W. S. Ahn, *Chem. Eng. J.*, 2016, **283**, 184–192.

70 S. H. Xiong, X. Fu, L. Xiang, G. Yu, J. P. Guan, Z. G. Wang, Y. Du, X. Xiong and C. Y. Pan, *Polym. Chem.*, 2014, **5**, 3424–3431.

71 S. K. Das, X. B. Wang and Z. P. Lai, *Microporous Mesoporous Mater.*, 2018, **255**, 76–83.

72 E. Troschke, S. Grätz, T. Lübken and L. Borchardt, *Angew. Chem., Int. Ed.*, 2017, **56**, 6859–6863.

73 S. He, Q. Rong, H. Niu and Y. Cai, *Chem. Commun.*, 2017, **53**, 9636–9639.

74 D. Kaleeswaran, R. Antony, A. Sharma, A. Malani and R. Murugavel, *ChemPlusChem*, 2017, **82**, 1253–1265.

75 L. Q. Xu, S. Y. Ding, J. M. Liu, J. L. Sun, W. Wang and Q. Y. Zheng, *Chem. Commun.*, 2016, **52**, 4706–4709.

76 M. G. Schwab, B. Fassbender, H. W. Spiess, A. Thomas, X. L. Feng and K. Mullen, *J. Am. Chem. Soc.*, 2009, **131**, 7216–7217.

77 W. Zhang, L. G. Qiu, Y. P. Yuan, A. J. Xie, Y. H. Shen and J. F. Zhu, *J. Hazard. Mater.*, 2012, **221**, 147–154.

78 A. Halder, S. Kandambeth, B. P. Biswal, G. Kaur, N. C. Roy, M. Addicoat, J. K. Salunke, S. Banerjee, K. Vanka, T. Heine, S. Verma and R. Banerjee, *Angew. Chem., Int. Ed.*, 2016, **55**, 7806–7810.

79 H. L. Qian, C. Dai, C. X. Yang and X. P. Yan, *ACS Appl. Mater. Interfaces*, 2017, **9**, 24999–25005.

80 R. Gomes, P. Bhanja and A. Bhaumik, *Chem. Commun.*, 2015, **51**, 10050–10053.

81 R. Gomes and A. Bhaumik, *RSC Adv.*, 2016, **6**, 28047–28054.

82 V. Sadhasivam, R. Balasaravanan, C. Chithiraikumar and A. Siva, *ChemistrySelect*, 2017, **2**, 1063–1070.

83 P. Puthiaraj and K. Pitchumani, *Chem.–Eur. J.*, 2014, **20**, 8761–8770.

84 T. T. Liu, X. Y. Hu, Y. F. Wang, L. Y. Meng, Y. N. Zhou, J. X. Zhang, M. Chen and X. M. Zhang, *J. Photochem. Photobiol., B*, 2017, **175**, 156–162.

85 N. Xu, R. L. Wang, D. P. Li, X. Meng, J. L. Mu, Z. Y. Zhou and Z. M. Su, *Dalton Trans.*, 2018, **47**, 4191–4197.

86 X. H. Guo, Y. Tian, M. C. Zhang, Y. Li, R. Wen, X. Li, X. F. Li, Y. Xue, L. J. Ma, C. Q. Xia and S. J. Li, *Chem. Mater.*, 2018, **30**, 2299–2308.

87 A. K. Sekizkardes, S. Altarawneh, Z. Kahveci, T. İslamoğlu and H. M. El-Kaderi, *Macromolecules*, 2014, **47**, 8328–8334.

88 J. Liu, K. K. Yee, K. K. W. Lo, K. Y. Zhang, W. P. To, C. M. Che and Z. T. Xu, *J. Am. Chem. Soc.*, 2014, **136**, 2818–2824.

89 P. Wen, C. Y. Zhang, Z. G. Yang, R. Dong, D. M. Wang, M. J. Fan and J. Q. Wang, *Tribol. Int.*, 2017, **111**, 57–65.

90 S. Gopi and M. Kathiresan, *Polymer*, 2017, **109**, 315–320.

91 H. Y. Zhao, Z. Jin, H. M. Su, X. F. Jing, F. X. Sun and G. S. Zhu, *Chem. Commun.*, 2011, **47**, 6389–6391.

92 C. Y. Bai, M. C. Zhang, B. Li, Y. Tian, S. Zhang, X. S. Zhao, Y. Li, L. Wang, L. J. Ma and S. J. Li, *J. Hazard. Mater.*, 2015, **300**, 368–377.

93 P. Puthiaraj and K. Pitchumani, *Green Chem.*, 2014, **16**, 4223–4233.

94 H. A. Patel, F. Karadas, J. Byun, J. Park, E. Deniz, A. Canlier, Y. Jung, M. Atilhan and C. T. Yavuz, *Adv. Funct. Mater.*, 2013, **23**, 2270–2276.

95 Y. L. Luo, B. Y. Li, L. Y. Liang and B. E. Tan, *Chem. Commun.*, 2011, **47**, 7704–7706.

96 T. Wang, R. Xue, H. Q. Chen, P. L. Shi, X. Lei, Y. L. Wei, H. Guo and W. Yang, *New J. Chem.*, 2017, **41**, 14272–14278.

97 Y. Z. Liao, J. Weber and C. F. J. Faul, *Macromolecules*, 2015, **48**, 2064–2073.

98 X. Zhu, S. H. An, Y. Liu, J. Hu, H. L. Liu, C. C. Tian, S. Dai, X. J. Yang, H. L. Wang, C. W. Abney and S. Dai, *AIChE J.*, 2017, **63**, 3470–3478.

99 A. Modak, M. Pramanik, S. Inagaki and A. Bhaumik, *J. Mater. Chem. A*, 2014, **2**, 11642–11650.

100 S. Ren, R. Dawson, A. Laybourn, J.-x. Jiang, Y. Khimyak, D. J. Adams and A. I. Cooper, *Polym. Chem.*, 2012, **3**, 928–934.

101 Y. Zhang, A. Sigen, Y. Zou, X. Luo, Z. Li, H. Xia, X. Liu and Y. Mu, *J. Mater. Chem. A*, 2014, **2**, 13422–13430.

102 Z. Xiang and D. Cao, *Macromol. Rapid Commun.*, 2012, **33**, 1184–1190.

103 Z. Xiang, D. Cao, L. Huang, J. Shui, M. Wang and L. Dai, *Adv. Mater.*, 2014, **26**, 3315–3320.

104 K. Gontarczyk, W. Bury, J. Serwatowski, P. Wiecinski, K. Wozniak, K. Durka and S. Lulinski, *ACS Appl. Mater. Interfaces*, 2017, **9**, 31129–31141.

105 S. Y. Yu, J. Mahmood, H. J. Noh, J. M. Seo, S. M. Jung, S. H. Shin, Y. K. Im, I. Y. Jeon and J. B. Baek, *Angew. Chem., Int. Ed.*, 2018, **57**, 8438–8442.

106 M.-S. Kim, C. S. Phang, Y. K. Jeong and J. K. Park, *Polym. Chem.*, 2017, **8**, 5655–5659.

107 K. W. Wang, L. M. Yang, X. Wang, L. P. Guo, G. Cheng, C. Zhang, S. B. Jin, B. Tan and A. Cooper, *Angew. Chem., Int. Ed.*, 2017, **56**, 14149–14153.

108 M. Liu, Q. Huang, S. Wang, Z. Li, B. Li, S. Jin and B. Tan, *Angew. Chem.*, 2018, **57**, 11968–11972.

109 M. Y. Liu, K. Jiang, X. Ding, S. L. Wang, C. X. Zhang, J. Liu, Z. Zhan, G. Cheng, B. Y. Li, H. Chen, S. B. Jin and B. Tan, *Adv. Mater.*, 2019, **31**, 1807865.

110 M. Dusselier and M. E. Davis, *Chem. Rev.*, 2018, **118**, 5265–5329.

111 L. J. Kong, J. Zhu, W. Shuang and X. H. Bu, *Adv. Energy Mater.*, 2018, **8**, 1801515.

112 Y. Fu, Z. Q. Wang, S. Z. Li, X. M. He, C. Y. Pan, J. Yan and G. P. Yu, *ACS Appl. Mater. Interfaces*, 2018, **10**, 36002–36009.

113 L. Hao, S. S. Zhang, R. J. Liu, J. Ning, G. J. Zhang and L. J. Zhi, *Adv. Mater.*, 2015, **27**, 3190–3195.

114 O. Buyukcakir, S. H. Je, S. N. Talapaneni, D. Kim and A. Coskun, *ACS Appl. Mater. Interfaces*, 2017, **9**, 7209–7216.

115 S. Mukherjee, M. Das, A. Manna, R. Krishna and S. Das, *Chem. Mater.*, 2019, **31**, 3929–3940.

116 K. Wang, H. Huang, D. Liu, C. Wang, J. Li and C. Zhong, *Environ. Sci. Technol.*, 2016, **50**, 4869–4876.

117 X. Jiang, P. Wang and J. J. Zhao, *J. Mater. Chem. A*, 2015, **3**, 7750–7758.

This journal is © The Royal Society of Chemistry 2019

J. Mater. Chem. A, 2019, **7**, 22848–22870 | 22869

118 X. Zhu, C. C. Tian, S. M. Mahurin, S. H. Chai, C. M. Wang, S. Brown, G. M. Veith, H. M. Luo, H. L. Liu and S. Dai, *J. Am. Chem. Soc.*, 2012, **134**, 10478–10484.

119 X. Liu, H. Li, Y. Zhang, B. Xu, A. Sigen, H. Xia and Y. Mu, *Polym. Chem.*, 2013, **4**, 2445–2448.

120 A. Bhunia, I. Boldog, A. Möller and C. Janiak, *J. Mater. Chem. A*, 2013, **1**, 14990–14999.

121 S. Hug, M. B. Mesch, H. Oh, N. Popp, M. Hirscher, J. Senker and B. V. Lotsch, *J. Mater. Chem. A*, 2014, **2**, 5928–5936.

122 S. Dey, A. Bhunia, D. Esquivel and C. Janiak, *J. Mater. Chem. A*, 2016, **4**, 6259–6263.

123 L. M. Tao, F. Niu, J. G. Liu, T. M. Wang and Q. H. Wang, *RSC Adv.*, 2016, **6**, 94365–94372.

124 K. Yuan, C. Liu, J. Han, G. Yu, J. Wang, H. Duan, Z. Wang and X. Jian, *RSC Adv.*, 2016, **6**, 12009–12020.

125 S. K. Das, X. Wang, M. M. Ostwal and Z. Lai, *Sep. Purif. Technol.*, 2016, **170**, 68–77.

126 X. Zhu, C. Tian, G. M. Veith, C. W. Abney, J. r. m. Dehaudt and S. Dai, *J. Am. Chem. Soc.*, 2016, **138**, 11497–11500.

127 K. Park, K. Lee, H. Kim, V. Ganesan, K. Cho, S. K. Jeong and S. Yoon, *J. Mater. Chem. A*, 2017, **5**, 8576–8582.

128 S. Dey, A. Bhunia, H. Breitzke, P. B. Groszewicz, G. Buntkowsky and C. Janiak, *J. Mater. Chem. A*, 2017, **5**, 3609–3620.

129 S. Gu, J. Guo, Q. Huang, J. He, Y. Fu, G. Kuang, C. Pan and G. Yu, *Macromolecules*, 2017, **50**, 8512–8520.

130 B. Guo, C. Wu, Q. Su, Z. Liu, X. Li, G. Li and Q. Wu, *Mater. Lett.*, 2018, **221**, 236–239.

131 L. Shao, Y. Li, J. Huang and Y.-N. Liu, *Ind. Eng. Chem. Res.*, 2018, **57**, 2856–2865.

132 D. M. D'Alessandro, B. Smit and J. R. Long, *Angew. Chem., Int. Ed.*, 2010, **49**, 6058–6082.

133 K. Yuan, C. Liu, L. Zong, G. Yu, S. Cheng, J. Wang, Z. Weng and X. Jian, *ACS Appl. Mater. Interfaces*, 2017, **9**, 13201–13212.

134 Y. Zhao, K. X. Yao, B. Teng, T. Zhang and Y. Han, *Energy Environ. Sci.*, 2013, **6**, 3684–3692.

135 S. Wu, Y. Liu, G. Yu, J. Guan, C. Pan, Y. Du, X. Xiong and Z. Wang, *Macromolecules*, 2014, **47**, 2875–2882.

136 M. Sevilla, P. Valle-Vigon and A. B. Fuertes, *Adv. Funct. Mater.*, 2011, **21**, 2781–2787.

137 M. G. Rabbani, A. K. Sekizkardes, O. M. El-Kadri, B. R. Kaafarani and H. M. El-Kaderi, *J. Mater. Chem.*, 2012, **22**, 25409–25417.

138 D. E. Demirocak, M. K. Ram, S. S. Srinivasan, D. Y. Goswami and E. K. Stefanakos, *J. Mater. Chem. A*, 2013, **1**, 13800–13806.

139 P. Puthiaraj, S.-M. Cho, Y.-R. Lee and W.-S. Ahn, *J. Mater. Chem. A*, 2015, **3**, 6792–6797.

140 A. Myers and J. M. Prausnitz, *AIChE J.*, 1965, **11**, 121–127.

141 S. Hug, L. Stegbauer, H. Oh, M. Hirscher and B. V. Lotsch, *Chem. Mater.*, 2015, **27**, 8001–8010.

142 X. Fu, Y. Zhang, S. Gu, Y. Zhu, G. Yu, C. Pan, Z. Wang and Y. Hu, *Chem.–Eur. J.*, 2015, **21**, 13357–13363.

143 M. Saleh, S. B. Baek, H. M. Lee and K. S. Kim, *J. Phys. Chem. C*, 2015, **119**, 5395–5402.

144 R. Dawson, A. I. Cooper and D. J. Adams, *Polym. Int.*, 2013, **62**, 345–352.

145 S. K. Das, X. Wang, M. M. Ostwal, Y. Zhao, Y. Han and Z. Lai, *Chem. Eng. Sci.*, 2016, **145**, 21–30.

146 S. K. Das, X. Wang and Z. Lai, *Microporous Mesoporous Mater.*, 2018, **255**, 76–83.

147 S. Dey, A. Bhunia, I. Boldog and C. Janiak, *Microporous Mesoporous Mater.*, 2017, **241**, 303–315.

148 K. Wang, Y. Tang, Q. Jiang, Y. Lan, H. Huang, D. Liu and C. Zhong, *J. Energy Chem.*, 2017, **26**, 902–908.

149 P. M. Mathias, R. Kumar, J. D. Moyer, J. M. Schork, S. R. Srinivasan, S. R. Auvil and O. Talu, *Ind. Eng. Chem. Res.*, 1996, **35**, 2477–2483.

150 Y. J. Lee, S. N. Talapaneni and A. Coskun, *ACS Appl. Mater. Interfaces*, 2017, **9**, 30679–30685.

151 Y. S. Bae and R. Q. Snurr, *Angew. Chem., Int. Ed.*, 2011, **50**, 11586–11596.

152 G. Tuci, M. Pilaski, H. Ba, A. Rossin, L. Luconi, S. Caporali, C. Pham-Huu, R. Palkovits and G. Giambastiani, *Adv. Funct. Mater.*, 2017, **27**, 1605672.

153 S. Nandi, U. Werner-Zwanziger and R. Vaidhyanathan, *J. Mater. Chem. A*, 2015, **3**, 21116–21122.

154 C. Gu, D. Liu, W. Huang, J. Liu and R. Yang, *Polym. Chem.*, 2015, **6**, 7410–7417.

155 A. Modak, M. Pramanik, S. Inagaki and A. Bhaumik, *J. Mater. Chem. A*, 2014, **2**, 11642–11650.

156 S. M. Kuznicki, V. A. Bell, S. Nair, H. W. Hillhouse, R. M. Jacubinas, C. M. Braunbarth, B. H. Toby and M. Tsapatsis, *Nature*, 2001, **412**, 720–724.

157 G. Wang, K. Leus, S. Zhao and P. Van Der Voort, *ACS Appl. Mater. Interfaces*, 2017, **10**, 1244–1249.

158 J. C. Wang and S. Kaskel, *J. Mater. Chem.*, 2012, **22**, 23710–23725.

159 J. Liu, X. Liu, Y. Sun, C. Sun, H. Liu, L. A. Stevens, K. Li and C. E. Snape, *Adv. Sustainable Syst.*, 2018, **2**, 1700115.

160 P. Puthiaraj and W.-S. Ahn, *J. Energy Chem.*, 2017, **26**, 965–971.

161 K. K. Wang, H. L. Huang, D. H. Liu, C. Wang, J. P. Li and C. L. Zhong, *Environ. Sci. Technol.*, 2016, **50**, 4869–4876.

162 Z. Z. Yang, S. Wang, Z. H. Zhang, W. Guo, K. C. Jie, M. I. Hashim, O. S. Miljanic, D. E. Jiang, I. Popovs and S. Dai, *J. Mater. Chem. A*, 2019, **7**, 17277–17282.

163 S. Mukherjee, M. Das, A. Manna, R. Krishna and S. Das, *J. Mater. Chem. A*, 2019, **7**, 1055–1068.

164 M. R. Liebl and J. Senker, *Chem. Mater.*, 2013, **25**, 970–980.

165 Y. Fu, Z. Wang, X. Fu, J. Yan, C. Liu, C. Pan and G. Yu, *J. Mater. Chem. A*, 2017, **5**, 21266–21274.